

Optimisation of Natural Circulation Boilers during Warm Start-Up

A mathematical model describing the dynamic phase
transition of water

Kasper Gram Bilde

Energy Technology, TEPE4-1001, June 2019

Master's Thesis



Copyright © Aalborg University 2019

The mathematical model is developed using MATLAB R2018b with no additional packages. The model developed utilises the built-in solvers.



Energy Technology
Aalborg University
<http://www.aau.dk>

AALBORG UNIVERSITY
STUDENT REPORT

Title:

Optimisation of Natural Circulation Boilers during Warm Start-Up

Theme:

Master's Thesis

Project Period:

Spring Semester 2019

Project Group:

TEPE4-1001

Participant(s):

Kasper Gram Bilde

Supervisor(s):

Kim Sørensen
Thomas Condra

Copies: 1

Page Numbers: 71

Date of Completion:

May 31, 2019

Abstract:

Performing a start-up of a warm boiler is a difficult procedure, since the water inside the tubes are close to saturation. During the start-up, warm air is purged through the boiler, causing rapid boiling in both the evaporator and economiser which results in a high water level in the steam drum. A mathematical model describing the dynamic performance of a natural circulation boiler is presented. The geometry of the boiler is simplified and discretized in one dimension. During boiling in the evaporator and economiser steam is produced which displaces the water in the evaporator tubes, resulting in a high water level in the steam drum. A correlation is presented for the relative starting pressure and the relative volume of water occupying the steam drum. Depending on the maximum allowable water level, a minimum starting pressure can be determined and high water levels can thereby be limited.

The content of this report is freely available, but publication (with reference) may only be pursued due to agreement with the author.

Executive Summary

In this thesis, a mathematical model describing the dynamic performance of a natural circulation boiler during a warm start-up is presented. The complex geometry of the natural circulation boiler is simplified to include the steam drum, the downcomer-riser loop, superheaters and economisers. The flue gas passing through the components couples the different heating surfaces.

When a plant is shut down, the system cools down, essentially following the saturation line, as the pressure decreases. When the plant is started again, a small amount of heat applied results in boiling in both the evaporator and economiser. When boiling occurs, the steam produced displaces the water resulting in an increased water level in the steam drum. During a warm start-up, the circulation of water is low, since the density difference between the inlet of the downcomer and the outlet of the evaporator is small. When boiling occurs the density difference rapidly becomes larger, resulting in a significantly increased flow. This phenomenon is observed at Aalborg Energie Teknik A/S, where the plant is sometimes shut down for safety reasons when a warm start-up is performed.

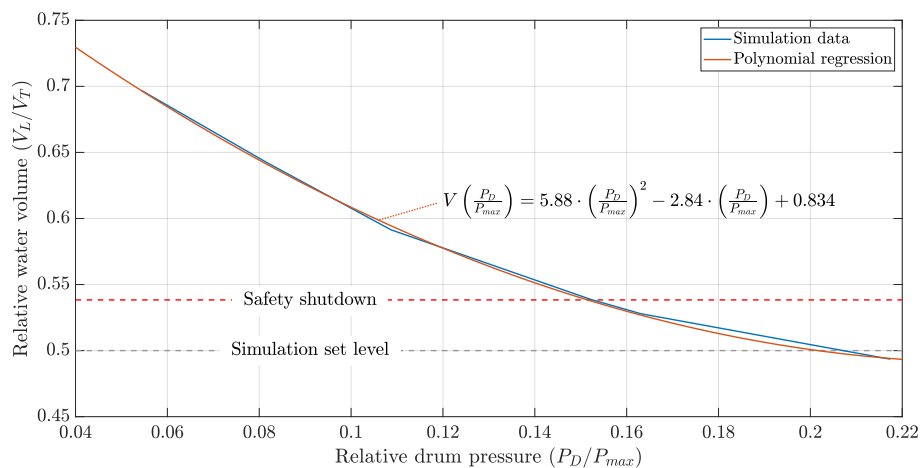


Figure 1: Relative water volume occupying the steam drum as a function of the relative starting pressure of the system. The safety shutdown is marked as +55 mm above the desired water level.

The mathematical model developed, is used to find a correlation describing the maximum water level in the steam drum as a function of the initial starting pressure. The relative water volume occupying the steam drum as a function of the relative starting pressure is seen in Fig. 1. In order to limit the water level in the steam drum, the correlation can be used as a reference to achieve a maximum water level which is within the limit.

Preface

The thesis is written by Kasper Gram Bilde at Aalborg University during the spring semester of 2019. This is the Master's project for M.Sc. in "*Thermal Energy and Process Engineering*" accounting for a total of 30-ECTS points. The project is carried out as an extension of the work done during an internship at Aalborg Energie Teknik A/S. During development of the model discussion and feedback have been given by the employees at Aalborg Energie Teknik A/S, Aalborg, Denmark.

Prerequisites

A good understanding of mathematics, physics and thermodynamics is needed to understand the contents of this thesis.

Reading Guidance

Throughout this thesis the literature is cited using their alphabetical order in the bibliography list, e.g. [15]. The bibliography is found in the end of the thesis, where the cited literature is listed in an alphabetical order. The scientific articles used are denoted by the name of the author(s), year of publishing, title, publisher, volume and *doi* number. Web pages are denoted with the direct web link and the date of the last visit. If the web page has been removed or changed, a copy of the web page can be found in the attached zip-folder.

Throughout the thesis figures, equations and tables have been numbered according to their chapter and appearance. For example the numbering of Fig. 4.1. The first number is a chapter reference and the second number is the figure number in the given chapter.

The nomenclature is found after the table of contents. The nomenclature contains abbreviations, dimensionless numbers, symbols and subscripts used in the thesis along with a description and the SI-unit. All pressures are denoted as the absolute pressure.

This thesis is uploaded as a duplex print version, and chapters therefore begin on the right-hand side. Empty pages might occur throughout the thesis.

Applied Software

The mathematical model is developed using MATLAB R2018b where the built-in solvers and functions are utilised. There is used no additional packages for the model developed. MATLAB is also used for post-processing and visualisation of the data given by the mathematical model.

Acknowledgements

A special thanks to Aalborg Energie Teknik A/S for the assistance in this project work. The practical knowledge gained during the internship and the discussion had during this thesis has been very valuable for the work.

Thesis Structure

The structure of the thesis is visually seen in Fig. 2.

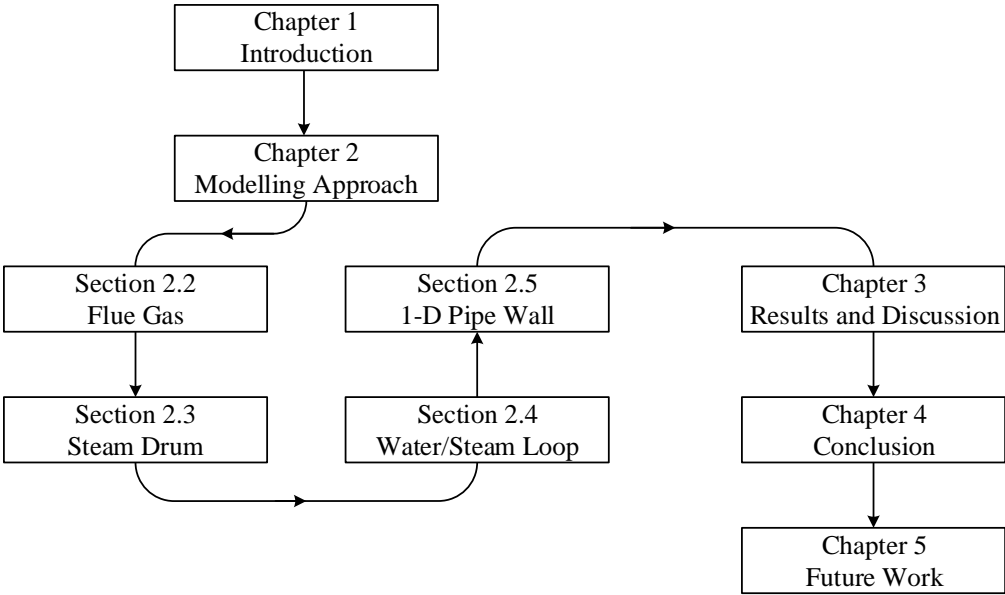


Figure 2: Overall structure of the thesis.

Contents

| | | |
|----------|---|-----------|
| 1 | Introduction | 1 |
| 1.1 | State of the art review | 4 |
| 1.2 | Scope of Thesis | 6 |
| 1.2.1 | Problem Formulation | 7 |
| 1.2.2 | Assumptions and Limitations | 7 |
| 2 | Modelling Approach | 9 |
| 2.1 | Simplification of Geometry | 10 |
| 2.2 | Modelling of the Flue Gas | 11 |
| 2.3 | Modelling of Steam Drum | 13 |
| 2.3.1 | Differential Equations for Steam Drum | 13 |
| 2.3.2 | Algebraic Equations for Steam Drum | 14 |
| 2.4 | Modelling of Water/Steam Loop | 16 |
| 2.4.1 | Natural Circulation Loop | 17 |
| 2.4.2 | Economiser | 21 |
| 2.4.3 | Superheaters | 23 |
| 2.5 | Modelling of Tube Wall | 23 |
| 2.6 | Dynamic Instabilities | 24 |
| 2.6.1 | Pressure-Drop Oscillations | 25 |
| 2.6.2 | Acoustic Oscillations | 25 |
| 2.6.3 | Thermal Oscillations | 25 |
| 2.6.4 | Density Wave Oscillations | 26 |
| 2.7 | Chapter Summary | 28 |
| 3 | Results and Discussion | 29 |
| 3.1 | Initialisation | 29 |
| 3.2 | Simulation Results | 30 |
| 3.2.1 | Mass Fraction of Steam | 31 |
| 3.2.2 | Mass Flow of Water and Steam | 32 |
| 3.2.3 | Water Level of Steam Drum | 36 |
| 3.3 | High Water Levels in Practice | 39 |

| | |
|--|-----------|
| 4 Conclusion | 41 |
| 5 Future Work | 43 |
| Bibliography | 45 |
| Appendices | 47 |
| A Basic Theory | 49 |
| A.1 Dynamic Modelling Approach | 49 |
| A.1.1 Conservation of Mass | 49 |
| A.1.2 Conservation of Energy | 50 |
| A.2 Conservation of Momentum | 51 |
| B Theory of Two-Phase Flow | 55 |
| B.1 Pressure loss in a homogeneous two-phase mixture | 56 |
| B.2 Heat transfer in two-phase flows | 59 |
| C Flue Gas Properties | 61 |
| D Mathematical Model of Natural Circulation Biomass Boilers during Start-Up | 63 |

Nomenclature

Symbols

| Symbol | Unit | Description |
|-----------|---------------------|--------------------------------------|
| A | m^2 | Area |
| AF | kg/kg | Air-to fuel ratio |
| C | - | Coefficient |
| c_p | J/kg·K | Specific heat capacity |
| D | m | Diameter |
| f | - | Darcy friction factor |
| G | kg/s·m ² | Mass flux |
| g | m/s ² | Gravitational acceleration |
| H | J | Enthalpy |
| h | W/m ² ·K | Convective heat transfer coefficient |
| h | J/kg | Specific enthalpy |
| k | W/m·K | Thermal conductivity |
| K_L | - | Minor pressure loss coefficient |
| L | m | Length |
| M | kg | Mass |
| \dot{m} | kg/s | Mass flow |
| P | Pa | Pressure |
| \dot{Q} | W | Heat flow |
| \dot{q} | W/m ² | Heat flux |
| T | K | Temperature |
| V | m ³ | Volume |
| v | m/s | Velocity |
| x | kg/kg | Steam mass fraction |

Greek symbols

| Symbol | Unit | Description |
|------------|----------------------------------|---------------------------|
| ϵ | m | Surface roughness |
| λ | kg/kg | Excess air ratio |
| μ | Pa·s | Dynamic viscosity |
| ν | m ³ /kg | Specific volume |
| ρ | kg/m ³ | Density |
| σ | W/m ² ·K ⁴ | Stefan-Boltzmann constant |
| θ | rad | Angle |

Subscripts

| Subscript | Description | Subscript | Description |
|-----------|---------------|-----------|----------------|
| 1P | Single phase | L | Liquid |
| 2P | Two-phase | LD | Liquid in drum |
| A | Acceleration | lg | Latent heat |
| F | Friction | S | Surface |
| fg | Flue gas | sat | Saturation |
| G | Gravitational | V | Vapour |
| H | Homogeneous | VD | Vapour in drum |
| i | Index | w | Wall |

Dimensionless numbers

| Symbol | Definition | Description |
|--------|---|-------------------|
| Bo | $\dot{q}/(\dot{G} \cdot h_{lg})$ | Boiling number |
| Co | $((1-x)/x)^{0.8} \cdot (\rho_V/\rho_L)^{0.5}$ | Convective number |
| Nu | $h \cdot L/k$ | Nusselt number |
| Pr | $c_p \cdot \mu/k$ | Prandtl number |
| Re | $\rho \cdot v \cdot D_n/\mu$ | Reynolds number |

Abbreviations

| Abbreviation | Description |
|--------------|------------------------------|
| AET | Aalborg Energie Teknik A/S |
| CFD | Computational Fluid Dynamics |
| DWO | Density Wave Oscillation |
| HHV | Higher Heating Value |
| UN | United Nations |

Chapter 1

Introduction

The United Nations (UN) has made 17 global sustainable development goals that have to be reached no later than 2030. All 17 goals have in common that they all improve the world we live in. Goal number 7 concerns the needs for affordable and clean energy [20]. 3 billion people worldwide do not have access to clean energy and the production of electricity comes from polluting sources. The desire for producing clean energy is of growing concern since the energy demand of the world is still increasing. In the European Union, a large percentage of the produced electricity still comes from fossil fuel sources. In Germany 40 % of the electricity produced comes from power plants burning coal. This is of major concern to the German people and the German government has in 2019 developed a plan to phase out these coal-fired power plants. The coal-fired power plants should be replaced by renewable sources in 2038 [27]. In Denmark, the coal-fired power plants produced 17 % of all electricity in 2017 [9], and the remaining coal-fired power plants should all be replaced with renewable sources by 2030 [21]. Besides the production of electricity, there is produced a large amount of energy to the industry in the form of steam. Steam is needed for a lot of different industries in order to produce the desired products.

In both Denmark and Germany other renewable solutions have to be found. One of the most popular methods, in the present time, of producing both electricity, heat and steam to the industry is to use biomass-fired boilers. Biomass is burned in a boiler and the chemical energy released from the burning biomass is transferred to the water and eventually, steam is produced. The steam can be used directly in the industry or it can be used in a steam turbine to produce electricity. The great advantage of biomass boilers is that CO₂-neutral energy is produced independent



Figure 1.1: UN's goal no. 7 regarding clean energy [20]

of sun and wind, meaning that the process can be controlled according to the energy demand.

Aalborg Energie Teknik A/S is a company located in Aalborg that designs, erects and develops biomass power plants and combined heat and power plants (CHP). The company has been developing large biomass boilers for the last 20 years and is currently delivering the largest power plant in the history of the company, which is seen in Fig. 1.2.

A typical biomass power plant consists of several groups of components that together produce steam. The waterside is best described by Fig. 1.3, where the water enters the economiser and is heated until saturation. It is then led to the steam drum where it is circulated through the evaporator. A mixture of water and steam leaves the evaporator and the steam drum separates the steam produced in the evaporator from the saturated water. The saturated steam in the steam drum is then led to the superheaters where the steam is



Figure 1.2: Erection site at Tilbury Green Power close to London [1].

superheated until the desired operating temperature is reached. When the desired temperature is reached, the steam is sent to the steam turbine where the energy stored in the steam is converted into electricity using a generator. The low-pressure steam at the outlet of the steam turbine is then condensed and is finally stored in the feedwater tank. When designing a natural circulation evaporator, the circulation of water is of great interest. It is important to ensure that sufficient cooling of the evaporator tubes is obtained, and especially that no burnout spots are experienced when operating the boiler. All of the biomass boilers erected by AET utilise natural circulation in the evaporation circulation loop. Natural circulation is where a pump is not installed in the evaporation circulation loop, and the circulation of water is, instead, driven by the density difference from the inlet of the downcomer to the outlet of the evaporator. The high-density water enters the downcomer and is then heated in the evaporator. As the water is heated, the density decreases and this density difference drives the fluid around the circulation loop. The circulation of water is therefore difficult to determine, especially during start-up where the operation of the boiler is highly dynamic. During evaporation of water, the steam void fraction is difficult to measure, since the temperature is constant throughout the two-phase regime. Even though it is difficult to measure the fraction of steam inside the tubes, there exists a number of methods for measuring the void fraction of steam. The measuring methods are not easily installed in large power plants

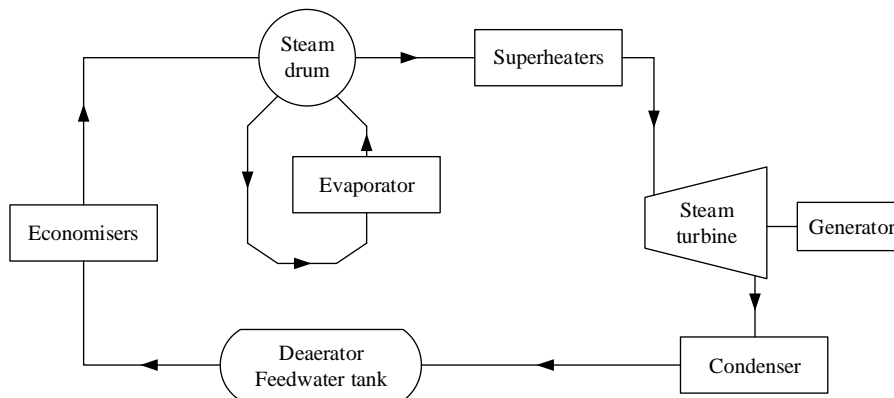


Figure 1.3: Simplified water/steam circuit in a typical biomass power plant

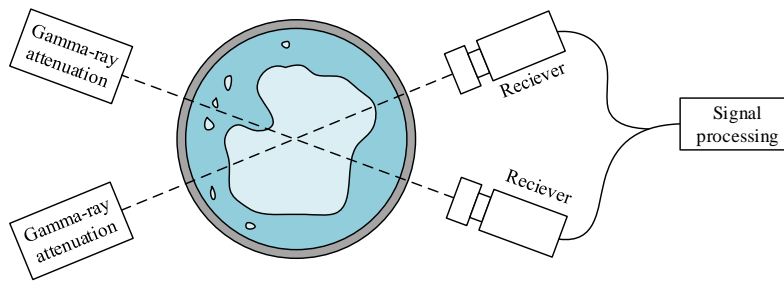


Figure 1.4: Gamma-ray attenuation system used to measure the void fraction of gas in a non-intrusive way [29].

due to the high temperatures and some methods are also flow intrusive. One of the most used methods in modern times is the gamma-ray attenuation or x-ray attenuation systems, where the intensity of the radioactive beam is measured as it passes through a tube [26] [29]. The intensity of the beam changes as it passes through gas or liquid and a void fraction can thereby be determined. This method is a non-intrusive method of measuring the void fraction of steam. In large power plants where the temperature is high ($T > 300^{\circ}\text{C}$), such equipment is not easily installed. The void fraction of steam is therefore often unknown to the plant operator, and the circulation number is only a design parameter.

Knowledge regarding the circulation of water as well as knowing where and when boiling occurs for a start-up procedure is valuable information for a plant operator. This information together with the pressure and temperature profile of the plant could improve the performance of the plant. When a plant is starting from cold conditions, the entire system needs to be heated. A simplified model describ-

ing the procedure of a cold start-up was developed during an internship at Aalborg Energie Teknik A/S [3]. The model developed is able to describe the circulation of water during the cold start-up procedure and it describes the dynamic evaporation of water. A paper has been submitted (April 2019) to the International Journal of Heat and Mass Transfer, with a focus on the rapid swelling inside the steam drum during a cold start-up, and the submitted paper can be found in App. D. In this work the model developed during the internship is expanded to handle a warm start-up procedure. When a plant is shut down from operating at full load, the entire plant cools down, theoretically, following the saturation line. The plant cools down as the temperature of the surroundings are colder than the plant. When the plant is cooled, the steam inside the system condenses and the pressure starts to decrease. When the plant is started, before the plant has reached thermal equilibrium with the surroundings, the water in the system is close to saturation and a small amount of heat results in steam being produced in the evaporator or economiser.

Before the burners are turned on during the start-up, the flue gas path is flushed with fresh air for safety reasons. This procedure is called *purging*. During purging, the hot air stored in the lowest part of the furnace is sent through the boiler, and it is sometimes experienced that boiling occurs in the economisers, since the economiser is also close to boiling during a warm start-up. If boiling in the economiser occurs, the liquid in the economiser is 'pushed' to the steam drum, and the plant is shut down for safety reasons due to high water levels in the steam drum.

In order to simulate the warm start-up procedure, the flue gas, economisers and superheaters are coupled to the existing model. The flue gas couples the heat surfaces within the boiler, as the flue gas is cooled when it passes through the boiler. The water/steam leaving the economisers enters the steam drum, and in order to simulate the flow leaving the economiser during boiler, this heating surface needs to be coupled to the evaporator-model. Before the flue gas reaches the economiser, it has to pass through the superheaters where an amount of heat is transferred to the steam inside the superheaters.

1.1 State of the art review

The dynamic performance of boilers has been the subject for a number of studies since the 1990s. Power plants rarely operate in a steady-state and therefore more comprehensive knowledge, regarding the dynamic operation of boilers, is of great interest. The studies typically focus on a plant operating at a certain load and then experiencing a change in load and analysing the change.

Elmegaard [8] developed a tool to simulate the dynamic performance of energy systems. The tool developed, named DNA, is a flexible tool that contains

a library of components. DNA is able to simulate most energy systems since the methodology used describes the mass, energy and momentum conservation for the individual components. The methodology is also used in this thesis for developing the mathematical model.

One of the most widely used models when describing the dynamic behaviour of the steam drum is the model developed by Åström and Bell [30]. The model is widely used because the authors propose a number of equations that are easily implemented into others model. The work focuses on the water level inside the steam drum and how to describe the dynamic behaviour of such a component. The limitations of the work are that the authors assume the water entering the evaporator is a saturated liquid, meaning that no subcooling of water is considered. Furthermore, it is assumed that the pressure changes instantaneously, thereby assuming the momentum equation can be solved in steady-state. The proposed model is able to describe the dynamic performance of a steam drum quite well.

Kim and Choi [16] expanded the work described by Åström and Bell [30] to take the condensation below the water level into account. The main focus is on the water level inside the steam drum and it is assumed that the water enters the evaporator as a saturated liquid. Since the focus is on the steam drum, the authors assume that the water entering the evaporator is saturated liquid, thereby limiting the work to not include subcooling of water. The proposed model is able to describe the dynamics of a steam drum quite accurately.

Sunil et al. [24] also use the drum model developed by Åström and Bell [30], but the authors have focused on improving the model for the downcomer-riser loop. The re-circulation loop is discretized into a number of 1-dimensional elements and the mass, energy and momentum equations are solved using the stability code, SPORTS, developed by Chatoorgoon [5]. The SPORTS code is a stability code developed to calculate the dynamic mass, energy and momentum equation. Chatoorgoon simplifies the equations by discretizing in 1-dimension and taking the forward difference approximation, thereby having simple non-linear terms to solve. Sunil et al. compare the simulation results obtained by the improved circulation model to Åström and Bell as well as a model developed by Bhambre et al. [2]. The results obtained with the improved circulation model shows an improvement compared to the two other models.

Sedic et al. [22] have developed a model describing the dynamics of a natural circulation boiler with a steam drum. The aim of the work was to develop a controller for the feedwater valve in order to control the water level inside the steam drum. The evaporator is discretized into 5 elements where the governing equations are solved as one-dimensional. The model is simulated for a plant operating at a given load and then experiencing a change in load. The model describes the control of the water level quite well, and it is assumed, from the governing equations, that this proposed model can also be used for simulating a start-up since

subcooling of water is taken into account.

Krüger et al. [17] optimised the start-up profiles with respect to the thermal stresses occurring in the thick-walled components such as the steam drum. The model is made with the assumption that the momentum equation can be solved in steady state as a function of the pressure drop only since the circulation is forced. The work focuses on the thermal stresses during start-up and it is concluded that an optimisation of the start-up can lead to a reduction of the start-up costs.

An extensive work is presented by Johansen et al. [13] regarding the dynamic modelling of once-through Benson boilers. The work describes the modelling procedure for such a boiler, where the water enters as subcooled water and exists as superheated steam in a single tube. The modelling procedure for such a system requires that the phase transition of water is taken into account. During a phase transition, dynamic instabilities are experienced, and Johansen et al. describe the procedures of how to dampen the pressure oscillations that occur when dynamic instabilities are experienced. To obtain a shorter computational time, Johansen et al. also proposes to use an interpolation table when calculating the properties of water and steam. The problem of how to resolve the saturation line is addressed. The model developed describes the dynamic phase transition of water in a Benson boiler where the circulation is forced.

The dynamic instabilities experienced when a fluid transitions to the two-phase regime have been the subject of a number of studies for both boiling and condensation systems. Kakac and Bon [14] collected and reviewed the different types of flow instabilities that occur during both steady-state and dynamic operation. The authors also reviewed the most popular methods to experimentally measure the dynamic instabilities.

The dynamic instability due to density wave oscillations (DWO) is determined experimentally in a natural circulation loop by Chen et. al [6]. The tests were performed in a macro-channel where heat is applied to a subcooled fluid and when the phase transition occurs a reverse flow is observed when the fluid has an unstable behaviour. The authors conclude that the flow starts to oscillate if the heat flux is larger than, or close to, the critical heat flux. If the heat flux is larger than the critical heat flux, the flow starts to move in the opposite direction due to the compressible volume in front of the fluid.

1.2 Scope of Thesis

In this project, a model for simulating a warm start-up for a natural circulation boiler is presented. During the warm start-up, boiling in both the evaporator and economiser is expected. The boiling of water results in a high water level in the steam drum, which is simulated using the model described in Chapter. 2. The model includes the physical transfer of heat from the flue gas to the fluid and is

able to simulate the dynamic phase transition of water. The phase transition is one of the main concerns of this work since the dynamic instabilities, introduced from the phase transition, are difficult to resolve. One of the main differences between previous studies and this study is that the momentum equation is solved as a differential equation for the water/steam side. The momentum equation makes the system of equations stiff since the pressure is able to propagate rapidly in the medium (order of speed of sound), whereas the continuity and energy equation changes much slower (order of seconds). The large time constant difference between the momentum equation and the other equations results in a stiff system of equations that is difficult to solve [11]. This is especially the case when the fluid transitions into the two-phase region, since the density changes to 1/100 of the initial density, very rapidly.

1.2.1 Problem Formulation

The working problem formulation for this thesis is:

How can high water levels inside the steam drum be limited during a warm start-up procedure?

With the following working questions:

1. Under what operating conditions does boiling occur in the economiser?
2. How can the water level inside the steam drum be controlled?

1.2.2 Assumptions and Limitations

To simulate the start-up procedure of such a large plant, assumptions and limitations have to be made. The assumptions and limitations applied for this work are stated in the following list.

Assumptions:

- The kinetic and potential energy contribution can be neglected for internal flow
- The two-phase water/steam mixture is a homogeneous mixture with no slip between the two phases.
- The complex boiler geometry can be simplified to the geometry presented in section 2.1.
- No condensation takes place inside the steam drum
- The temperature of the flue gas is uniformly distributed

Limitations:

- The water/steam and flue gas flow are only calculated in one dimension.
- Combustion of fuel is not taken into consideration
- Heat exchange between the flue gas and the water walls is neglected in the first and second pass (see Fig. 2.1).
- The superheating of steam is not the focus of this thesis, therefore little detail on this is presented.

Chapter 2

Modelling Approach

To model a biomass boiler dynamically during a start-up is a challenging task if no simplifications are made. To get a better understanding of why this is so, a more detailed description of the power plant is presented.

The main concept of a steam boiler is that fuel is burned and the heat released is transferred to the water in the system. The water is then evaporated and the steam produced is heated until the desired operating temperature is reached. To reach a high steam quality, steam boilers typically operate under high pressures. Some plants are operating under supercritical conditions, but the Tilbury Green Power plant delivers steam to a steam turbine at a pressure of 92 bar_a. The overall flow diagram for the flue gas and the water/steam circuit is seen in Fig. 2.1. The two fluids exchange heat in the combustion chamber and in the second and third pass of the boiler. In the furnace, the temperature of the flue gas is high, $T_{fg} \approx 1200^\circ\text{C}$, and the dominating heat transfer is thermal radiation. As the flue gas moves further into the boiler, the heat transfer due to convection starts to dominate due to the lower flue gas temperature. The water is initially stored in the feedwater tank where it is also deaerated. Air and other gasses that might be stored in the water is deaerated using steam that is produced in the process. When the water leaves the feedwater tank, it is led through the economisers where it is heated until saturation is reached when operating at full load.

When the plant is starting, the temperature of the water leaving the economiser is typically lower than the saturation temperature. The heated water leaves the economiser and enters the steam drum where it is evaporated in the circulation evaporation loop. The main purpose of the steam drum is to separate the saturated steam from the saturated water. The saturated steam leaving the steam drum is heated until the desired temperature in the superheaters located after the furnace. The steam turbine converts the energy stored in the high-temperature steam to mechanical energy and then, using a generator, into electrical energy. The water/steam loop, seen in Fig. 2.1, is, of course, simplified since the system is more

complex in practice. In practice preheaters, air preheaters and different heat exchangers are also installed. Furthermore, the steam produced is also used to heat different components of the system.

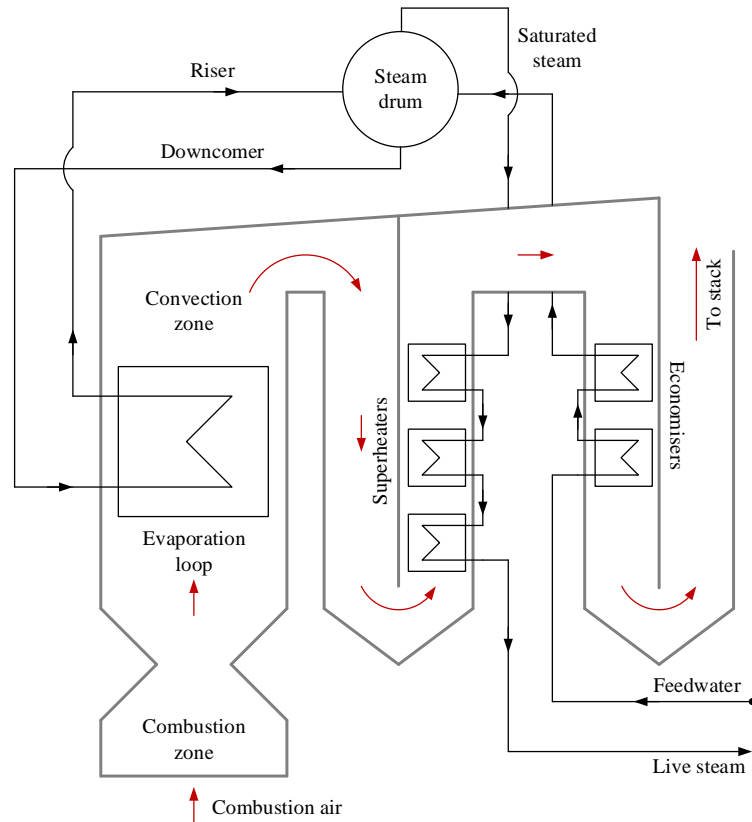


Figure 2.1: Overview of the path of the flue gas in the boiler as well as the water/steam circuit.

2.1 Simplification of Geometry

The geometry of the entire boiler is complex and in order to develop a model to describe the start-up procedure, the geometry needs to be simplified. The furnace, first-, and second pass are enclosed in water walls that make sure the walls of the boiler do not become damaged from the high-temperature flue gas. The water walls also serve as the evaporator/riser tubes. The temperature of the flue gas is highest in the furnace, and the main heat transfer to the water walls, therefore, occurs in the furnace. The heat transfer to the water walls in the first and second pass is therefore neglected in this work. Since the water walls in the second pass are neglected, the flue gas only transfers heat to the superheaters in this section.

The geometry of the furnace is also simplified so that the entire furnace is modelled as a rectangular shape as seen in Fig. 2.2. This also means that the narrow passage at the combustion zone seen in Fig. 2.1 is neglected. The evaporator is simplified to 300 straight parallel tubes. In practice, the evaporator tubes are of different length and shape since the tubes are bent to accommodate equipment sticking out of the boiler wall.

2.2 Modelling of the Flue Gas

The flue gas is initially the same temperature as the water to ensure the entire plant is in thermal equilibrium. During a regular start-up, the oil burners are used to heat the flue gas. As the gas is heated it transfers heat to the water walls in the furnace, and the heated flue gas is then transported to the first-, second-, and third pass where the heat is transferred to the superheaters and economisers. The furnace is discretized into a number of elements and the discretized elements are the same size as the element of the water walls. This is also seen in Fig. 2.2. The very first element is chosen as the combustion zone for the biomass burning on the grate. The oil burners are placed in the third element. This is also seen in Fig. 2.3. The combustion process is neglected in this work and a simple linear expression which is introduced instead. To calculate the mass flow of flue gas, the mass flow of fuel needs to be calculated first as seen in Eq. 2.1.

$$\dot{m}_{fuel} = \underbrace{\frac{\dot{Q}_{burner}}{LHV_{oil}}}_{\dot{m}_{oil}} + \underbrace{\frac{\dot{Q}_{biomass}}{LHV_{wood}}}_{\dot{m}_{wood}} \quad (2.1)$$

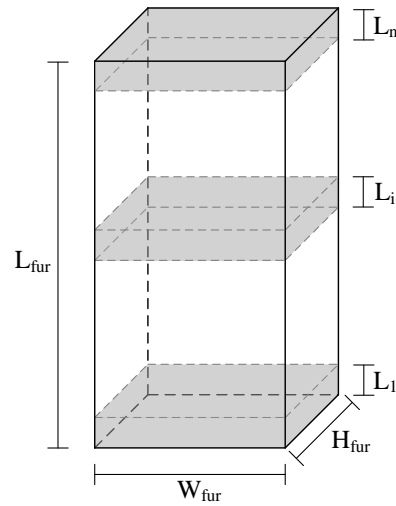


Figure 2.2: Furnace is discretized into n -elements.

Knowing the mass flow of fuel, the mass flow of flue gas can be calculated using a simplified combustion approach. Knowing the stoichiometric air-to-fuel ratio results in a stoichiometric combustion of fuel. During a typical combustion there is an excess air ratio and during the start-up the excess air ratio is larger than when the plant is operating a full load. Therefore the mass flow of flue gas can be calculated using Eq. 2.2.

$$\dot{m}_{fg} = \dot{m}_{oil} \cdot AF_{oil} \cdot \lambda_{oil} + \dot{m}_{wood} \cdot AF_{wood} \cdot \lambda_{wood} \quad (2.2)$$

The main heat transfer occurring in the furnace is due to thermal radiation and as the flue gas moves further into the boiler the heat transfer due to convection

starts to dominate. The heat transferred from the flue gas to the walls is calculated using Eq. 2.3.

$$\dot{Q}_{fg \rightarrow w} = \dot{Q}_{rad} + \dot{Q}_{conv} \quad (2.3)$$

The heat transfer due to radiation is calculated using Eq. 2.4. There are three contributions for the thermal radiation; one for the current element and then the flue gas is also transferring heat to the element above and below, as illustrated in Fig. 2.3. The thermal radiation to the element above is radiation through the top lid of the discretized element. The thermal radiation contribution to the above and below elements are seen in Eq. 2.5 and 2.6.

$$\dot{Q}_{rad} = \sigma \epsilon A_s \left(T_{fg,i}^4 - T_{w,i}^4 \right) \quad (2.4)$$

$$\dot{Q}_{rad,i-1} = \sigma \epsilon A_{s,lid} \left(T_{fg,i}^4 - T_{w,i-1}^4 \right) \quad (2.5)$$

$$\dot{Q}_{rad,i+1} = \sigma \epsilon A_{s,lid} \left(T_{fg,i}^4 - T_{w,i+1}^4 \right) \quad (2.6)$$

The convective heat transfer from the flue gas to the wall is calculated using Newton's law of cooling [4], as seen in Eq. 2.7.

$$\dot{Q}_{conv} = h_{fg} \cdot A_s \cdot (T_{fg,i} - T_{w,i}) \quad (2.7)$$

The heat transfer coefficient for the flue gas is calculated the Dittus-Boelter equation, seen in Eq. 2.8, which can also be applied for rectangular channels according to Cengel [4].

$$Nu = 0.023 \cdot Re^{0.8} \cdot Pr^{0.4} \quad (2.8)$$

The heat transfer coefficient is calculated using the same approach as for the internal tube flow, which is described in section 2.4. The transport- and thermal properties, needed to calculate the heat transfer coefficient, are calculated using the NASA polynomials and more information can be found in App. C.

Only the energy conservation equation is applied to the flue gas since the mass flow of the flue gas is calculated using a linear expression and is assumed constant in all the discretized elements. The state variable for the flue gas is temperature and the differential equation is seen in Eq. 2.9.

$$\frac{dT_{fg,i}}{dt} = \frac{\dot{m}_{fg} \cdot c_{p,i-1} \cdot T_{fg,i-1} - \dot{m}_{fg} \cdot c_{p,i} \cdot T_{fg,i} + \dot{Q}_{in} - \dot{Q}_{fg \rightarrow w}}{V_i \cdot \rho_{fg,i} \cdot c_{p,i}} \quad (2.9)$$

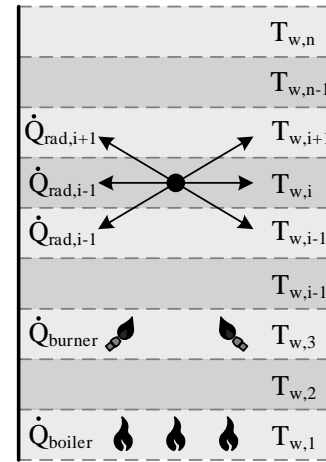


Figure 2.3: Radiation to below, current and top element. Firing location of burners and grate.

The heat input \dot{Q}_{in} is applied to the first and third element, as the grate is placed in the first element and the burners are placed in the third element, also seen in Fig. 2.3.

2.3 Modelling of Steam Drum

The steam drum is the vessel where water and steam are separated. During start-up, the steam drum is initially filled with water until a low water level is reached. This allows the water to expand when heated until the pressure can be increased. An overview of the steam drum is seen in Fig. 2.4. Feedwater is fed to the steam drum in order to maintain a desired water level inside the drum. The water/steam mixture produced in the riser tubes is separated in the cyclone when the mixture enters the steam drum. The saturated steam leaves the steam drum via the outlet tube and is then superheated in the superheaters.

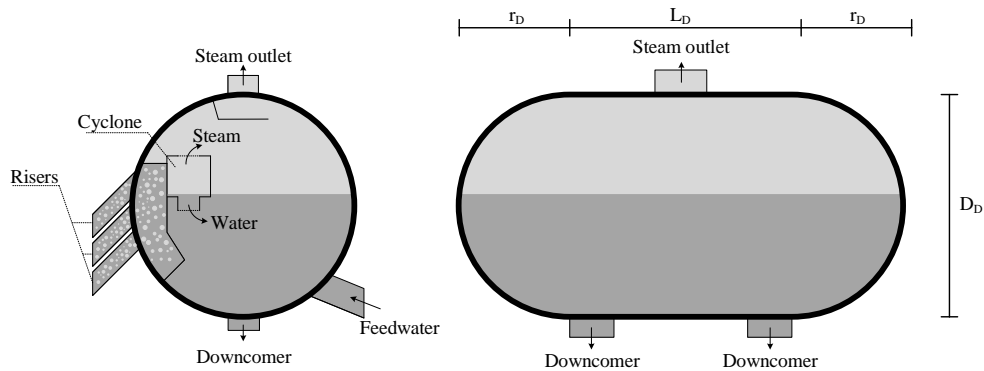


Figure 2.4: Side view and overview of a steam drum.

2.3.1 Differential Equations for Steam Drum

When modelling a steam drum during start-up, the liquid and gas phase have to be modelled separately. Therefore mass and energy differential conservation equations are applied to both the liquid and gas phases. During a cold start-up, there is initially no steam in the drum, since steam is first produced when the water has reached saturation. For a warm start-up procedure, it is assumed that volume, not occupied by water, is filled with saturated steam. The water/steam mixture is modelled using the homogeneous model [7], and steam cannot be produced before the liquid has reached saturation. The steam drum is modelled as a point, meaning no momentum can be stored in the steam drum.

Following the in- and outlet of the steam drum, the global mass and energy

differential equations are seen in Eqs. 2.10 and 2.11 respectively.

$$\frac{dM_D}{dt} = \dot{m}_{eco} + \dot{m}_r - \dot{m}_s - \dot{m}_{dc} \quad (2.10)$$

$$\frac{dH_D}{dt} = \dot{m}_{eco}h_{eco} + \dot{m}_r h_r - \dot{m}_s h_s - \dot{m}_{dc} h_{dc} \quad (2.11)$$

The conservation of mass and energy for the liquid phase are seen in Eqs. 2.12 and 2.13 and the conservation equations for the gas phase are seen in Eqs. 2.14 and 2.15.

$$\frac{dM_{LD}}{dt} = \dot{m}_{eco} + (1-x)\dot{m}_r - \dot{m}_{dc} \quad (2.12)$$

$$\frac{dH_{LD}}{dt} = \dot{m}_{fw}h_{fw} + (1-x)\dot{m}_r \cdot h_r - \dot{m}_{dc} \cdot h_{dc} + V_{LD} \frac{dP_D}{dt} \quad (2.13)$$

$$\frac{dM_{VD}}{dt} = x\dot{m}_r - \dot{m}_s \quad (2.14)$$

$$\frac{dH_{VD}}{dt} = x\dot{m}_r \cdot h_V - \dot{m}_s h_V + V_{VD} \frac{dP_D}{dt} \quad (2.15)$$

The mass flow of feedwater is controlled by the feedwater control valve, which is designed to maintain a desired water level. The feedwater specific enthalpy is a function of the heat transferred to the economisers, which is described in section 2.4.

The mass flow of steam leaving the steam drum is controlled by the main steam valve, which is designed to control the temperature gradient of the steam drum. In this thesis the main steam valve is assumed ideal, meaning steam can leave at any desired rate. The main steam valve is thereby modelled without the practical constraints of a real valve, e.g. a linearly controlled valve.

2.3.2 Algebraic Equations for Steam Drum

The thermal properties inside the steam drum are determined by the state variables, mass and enthalpy, and also using the knowledge that the two phases are separated.

The mass fraction of steam entering the steam drum is calculated using Eq. 2.16.

$$x = \frac{h_{evap,out} - h_L}{h_V - h_L} \quad (2.16)$$

From the equation it is seen that the mass fraction is allowed to be negative, since the water at the beginning of the simulation is subcooled, resulting in an outlet enthalpy less than the saturation enthalpy. Therefore the mass fraction has a minimum value of 0, as seen in Eq. 2.17.

$$x = \begin{cases} 0 & \text{for } h_{evap,out} < h_L \\ \text{Eq. 2.16} & \text{for } h_{evap,out} \geq h_L \end{cases} \quad (2.17)$$

The same applies to the enthalpy of the downcomers and riser, since the water is allowed to be subcooled.

$$h_r = \begin{cases} h_{evap,out} & \text{for } h_{evap,out} < h_L \\ h_L & \text{for } h_{evap,out} \geq h_L \end{cases} \quad (2.18)$$

$$h_{dc} = \begin{cases} h_D & \text{for } h_D < h_L \\ h_L & \text{for } h_D \geq h_L \end{cases} \quad (2.19)$$

The maximum allowable temperature gradient of the drum dictates the pressure gradient of the drum. At every time step a maximum pressure increase is calculated using Eq. 2.20.

$$\left. \frac{dP_D}{dt} \right|_{\max} = \frac{P_{sat}(T_D + \Delta T) - P_{sat}(T)}{\Delta t} \quad (2.20)$$

The maximum temperature gradient is a design parameter and for the Tilbury Green Power plant, the maximum temperature gradient is defined as:

$$\left. \frac{dT}{dt} \right|_{\max} = \frac{2.5 \text{ [K]}}{60 \text{ [s]}} \quad (2.21)$$

The maximum pressure gradient is also a function of the heat input. If too little heat is applied, the maximum temperature increase and the corresponding pressure increase cannot be achieved and the result is that no steam escapes the steam drum as a result of too little heat applied. Assuming no steam leaves the steam drum, the pressure is a function of the volume inside the steam drum, as seen in Eq. 2.22. The equation is solved iteratively since the volume of the liquid and gas phase is a function of the pressure. The sum of the volume of each phase is equal to the total volume of the steam drum.

$$V_D - [V_{LD}(P_D) + V_{VD}(P_D)] = 0 \quad (2.22)$$

The maximum allowable pressure gradient always limits the pressure in the system, and therefore the minimum pressure obtained by the two expressions is always chosen.

Depending on which pressure expression is used, the steam either leaves the drum or remains inside the drum to increase the pressure. The mass of steam leaving is simply the mass of steam that cannot be stored in the drum at the given drum pressure.

The feedwater controller is designed as a single element controller where only the water level inside the steam drum is controlling the valve. The feedwater flow is active when the actual water level inside the steam drum is lower than the

setpoint. An equation describing the single element controller for the feedwater flow is seen in Eq. 2.23.

$$\dot{m}_{fw} = \frac{L_{set} - L_{act}}{L_{set}} \cdot k_p \cdot \dot{m}_{fw,max} \quad (2.23)$$

Where k_p is a proportional gain value. The higher the gain value, the faster the set level is reached, and if the gain value is infinitely large, the controller is essentially an on-off controller. The actual water level inside the steam drum is calculated knowing the mass of liquid inside the drum, the thermal properties of water and the geometry of the steam drum. The volume occupied by the water inside the steam drum is calculated knowing the specific volume of the fluid in the steam drum, as seen in Eq. 2.24. The specific volume of the liquid depends on whether the liquid is saturated or not. When saturation is reached, the water is always saturated liquid.

$$V_{LD} = \begin{cases} M_{WD} \cdot v(P_D, h_D) & \text{for } h < h_L(P_D) \\ M_{WD} \cdot v_L(P_D) & \text{for } h \geq h_L(P_D) \end{cases} \quad (2.24)$$

Knowing the volume of the liquid inside the steam drum, the water level can be calculated using the geometry of steam drum as seen in Fig. 2.4, solving Eq. 2.25.

$$V_{LD} = L_D \underbrace{\left[r_D^2 \cos^{-1} \left(\frac{r_D - L_{act}}{r_D} \right) - (r_D - L_{act}) \sqrt{2r_D L_{act} - L_{act}^2} \right]}_{\text{Partially filled cylinder}} + \underbrace{\left[\pi L_{act}^2 r_D - \pi \frac{L_{act}^3}{3} \right]}_{\text{Partially filled sphere}} \quad (2.25)$$

2.4 Modelling of Water/Steam Loop

The water/steam side consists of several lumped components. The water is evaporated in the circulation loop, preheated in the economiser and superheated in the superheaters. In this section, the dynamic and algebraic equations for the water/steam side is presented starting with the circulation loop, followed by the economiser and finally the superheaters.

2.4.1 Natural Circulation Loop

The water is circulated using the density difference between the cold water entering the downcomer and the water/steam mixture exiting the evaporator. This method is widely used in large scale boilers since it eliminates the need to install a pump in the system. Biomass boilers are typically tall, which results in great conditions for natural circulation, due to the large height difference. For supercritical boilers or Benson boilers, there is most often installed a pump to control the start-up, because the operator would like to have a more controlled process. The natural circulation of water cannot be controlled and it is therefore important that it is properly designed. The natural circulation loop consists of a downcomer and an evaporator as seen in Fig. 2.5 and there is applied a system of differential equations to both the downcomer and the evaporator. The partial differential equations are discretized using the same procedure for both the downcomer and evaporator. More details on the derivation of the discretization can be found in App. A. As seen in Fig. 2.5, both the downcomer and evaporator are discretized into a number of one-dimensional elements.

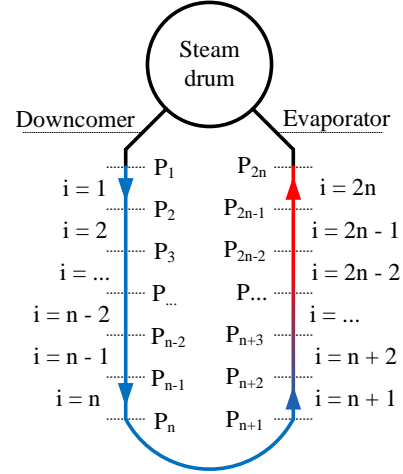


Figure 2.5: Natural circulation loop with discretization.

Differential Equations for Downcomer

For each downcomer element, the conservation of mass, energy and momentum is applied. The ODEs are solved in the centre of each element making it the mean value of the element. The pressures used to solve the momentum equation are interpolated pressure values, which is described in the following section. There is no heat applied to the downcomer sections, and the fluid is flowing in the same direction as gravity. The mass, energy and momentum differential equations are seen in Eqs. 2.26, 2.27 and 2.28 respectively.

$$\frac{dM_i}{dt} = \dot{m}_{i-1} - \dot{m}_i \quad (2.26)$$

$$\frac{dH_i}{dt} = \dot{m}_{i-1}h_{i-1} - \dot{m}_i h_i + V_i \frac{dP_i}{dt} \quad (2.27)$$

$$\frac{d\bar{v}_i}{dt} = \frac{P_i - P_{i+1} - \Delta P_i}{\bar{\rho}_i \cdot L_i} + \bar{v}_i \frac{v_{i-1} - v_i}{L_i} + g \quad (2.28)$$

Differential Equations for Evaporator

The conservation of mass, energy and momentum are also applied to each of the evaporator segments in the same way as the equations for the downcomer. The difference is that heat is applied to the evaporator and the fluid is flowing in the opposite direction of gravity. The differential conservation equations for mass, energy and momentum are seen in Eqs. 2.29, 2.30 and 2.31 respectively.

$$\frac{dM_i}{dt} = \dot{m}_{i-1} - \dot{m}_i \quad (2.29)$$

$$\frac{dH_i}{dt} = \dot{m}_{i-1}h_{i-1} - \dot{m}_i h_i + \dot{Q}_{f,i} + V_i \frac{dP_i}{dt} \quad (2.30)$$

$$\frac{d\bar{v}_i}{dt} = \frac{P_i - P_{i+1} - \Delta P_i}{\bar{\rho}_i \cdot L_i} + \bar{v}_i \frac{v_{i-1} - v_i}{L_i} - g \quad (2.31)$$

Algebraic Equations for Natural Circulation Loop

To solve the differential equations, a system of algebraic equations needs to be solved for each of the discretized elements. All thermal and transport properties of the fluid are calculated from the three state variables; mass, enthalpy and velocity. All properties are evaluated as mean values for each element and the pressure is then linearly interpolated to the in- and outlet of each element to solve the momentum equation.

The density for each element is evaluated using the mass and volume as seen in Eq. 2.32.

$$\bar{\rho}_i = \frac{M_i}{V_i} \quad (2.32)$$

The specific enthalpy of each element is needed to solve the energy conservation equation, but it is also necessary to calculate other thermal properties of the fluid. The specific enthalpy is calculated using Eq. 2.33.

$$\bar{h}_i = \frac{H_i}{M_i} \quad (2.33)$$

The pressure of each element is more difficult to calculate since it is a function of the thermal properties of the fluid. The pressure can be calculated knowing the density and enthalpy and applying the IAPWS-IF97 steam tables [25]. The problem with using density and enthalpy as variables when calculating the pressure is that the steam tables are very sensitive to changes in density. This is especially the case in the vicinity of the saturation line. Therefore an iterative solver with low convergence criteria is developed to ensure the pressure is correct. The pressure is then a function of the specific enthalpy and density as seen in Eq. 2.34.

$$\bar{P}_i = f(\bar{\rho}_i, \bar{h}_i) \quad (2.34)$$

From the mean pressure evaluated, the in- and outlet pressures of each element is linearly interpolated as seen in Eq. 2.35. It is assumed that the inlet pressure of the first element is known, which is also the case since it is dictated by the pressure in the steam drum.

$$P_{out,i} = 2 \cdot \bar{P}_i - P_{in,i} \quad (2.35)$$

The mass flow, used in the continuity and momentum equations, is calculated using Eq. 2.36. It is assumed that the cross sectional area of the tube does not change throughout the length.

$$\dot{m}_i = \bar{v}_i \cdot \bar{\rho}_i \cdot A_C \quad (2.36)$$

The internal pressure loss in the downcomer and evaporator is calculated using two different methods since the flow is either single phase or two-phase. For the single phase flow Eq. 2.37 is applied [4], but for the two-phase mixture this equation does not apply. The literature state different methods for solving the pressure loss in a two-phase mixture. The classical methods include flow frictional multipliers described by Collier and Thome [7] or separate models also described by Whalley [28]. In this work the two-phase mixture is assumed homogeneous meaning there is no slip between the liquid and gas phase, and then the pressure gradients also described by Whalley is applied. A derivation of the pressure gradient to explicit expression can be found in App. B.

$$\Delta P_{1P} = \left(f \cdot \frac{L_i}{D_i} + \sum_k K_L \right) \cdot \frac{1}{2} \cdot \bar{\rho}_i \cdot \bar{v}_i^2 \quad (2.37)$$

In the previous project, where the first stage of this model was developed, a pressure loss coefficient of $K_L = 1$ were found to be a suitable value and this is also used in this work [3]. The Darcy friction factor is usually calculated using the Colebrook-White equation as seen in Eq. 2.38.

$$\frac{1}{\sqrt{f}} = -2 \log \left(\frac{\epsilon}{3.7D_i} + \frac{2.51}{\text{Re} \sqrt{f}} \right) \quad (2.38)$$

The Colebrook-White equation is an implicit function and due to the computational time it takes to solve this implicit function another explicit expression were chosen. The Darcy friction factor is instead calculated using Haaland's explicit formula as seen in Eq. 2.39.

$$\frac{1}{\sqrt{f}} = -1.8 \log \left[\left(\frac{\epsilon/D_i}{3.7} \right)^{1.11} + \frac{6.9}{\text{Re}} \right] \quad (2.39)$$

Haaland's equation only applies for turbulent flow which is the case most of the simulated time, but during the initial start-up the flow is laminar. The flow is

assumed laminar when the Reynolds number is less than 4000. The Darcy friction factor is therefore calculated using the statements seen in Eq. 2.40.

$$f(\text{Re}) = \begin{cases} 64/\text{Re} & \text{for } \text{Re} < 4000 \\ \text{Eq. 2.39} & \text{for } \text{Re} \geq 4000 \end{cases} \quad (2.40)$$

The two-phase pressure loss is calculated using the two-phase frictional, gravitational and accelerational terms respectively as seen in Eq. 2.41.

$$\Delta P_{2P} = \Delta P_F + \Delta P_G + \Delta P_A \quad (2.41)$$

The pressure difference terms for friction, gravitation and acceleration are seen in Eqs. 2.42, 2.43 and 2.44 respectively. For the frictional term a homogeneous mixture density ρ_H is applied.

$$\Delta P_F = f \cdot \frac{L_i}{D_i} \cdot \frac{1}{2} \cdot \frac{\dot{G}^2}{\rho_H} \quad (2.42)$$

$$\Delta P_G = g \cdot \sin \theta \cdot \rho_L \cdot L_i \cdot \left(\frac{\ln(1 + X_0)}{X_0} \right) \quad (2.43)$$

$$\Delta P_A = \dot{G}^2 \cdot \frac{X_0}{\rho_L} \quad (2.44)$$

To calculate the energy transferred to the fluid from the tube wall, Newton's law of cooling is applied as seen in Eq. 2.45.

$$\dot{Q}_{f,i} = h_i \cdot A_s \cdot (T_{w,i} - T_{f,i}) \quad (2.45)$$

Where the heat transfer coefficient, h_i is calculated using Eq. 2.46 for single phase flow.

$$h_{1P} = \frac{\text{Nu} \cdot k_{f,i}}{D_H} \quad (2.46)$$

The Nusselt number is calculated using the Dittus-Boelter equation for circular tubes, as seen in Eq. 2.47.

$$\text{Nu} = 0.023 \cdot \text{Re}^{0.8} \cdot \text{Pr}^{0.4} \quad (2.47)$$

Where the Reynolds and Prandtl number is calculated using Eqs. 2.48 and 2.49 respectively.

$$\text{Re} = \frac{\bar{\rho}_i \bar{v} D_i}{\mu_i} \quad (2.48)$$

$$\text{Pr} = \frac{c_{p,i} \cdot \mu_i}{k_i} \quad (2.49)$$

It is a more difficult to calculate the heat transfer coefficient for a two-phase mixture. Different literature propose different methods for calculating the heat transfer coefficient and often a sufficient large heat transfer coefficient ($h_{2P} > 10000$ W/m²K) is chosen for simplicity. For this work a general correlation for vertical tubes proposed by Kandlikar [15], seen in Eq. 2.50, is chosen due to the simple term that is easy to implement in a model. More details can be found in App. B including the coefficients seen in Eq. 2.50.

$$h_{2P} = \underbrace{C_1 Co^{C_2} h_L}_{\text{Convective boiling term}} + \underbrace{C_3 Bo^{C_4} h_L}_{\text{Nucleate boiling term}} \quad (2.50)$$

The convective number, Co , and the boiling number, Bo , are seen in Eqs. 2.51 and 2.52 respectively.

$$Co = \left(\frac{1 - x_i}{x_i} \right)^{0.8} \left(\frac{\rho_V}{\rho_L} \right)^{0.5} \quad (2.51)$$

$$Bo = \frac{\dot{q}}{\dot{G} \cdot h_{lg}} \quad (2.52)$$

2.4.2 Economiser

The economiser is modelled using the same approach as for the evaporator. The economiser is located further downstream the flue gas flow, resulting in a colder flue gas reaching the economiser. The main task for the economiser is to preheat the water so that, essentially, saturated liquid enters the steam drum. During a start-up procedure, the economiser is filled with water which is heated. Until steam is produced and the feedwater controller requests a feedwater flow, there is no flow inside the economiser except for the flow due to the water expanding.

The economiser is essentially a heating surface with a number of parallel tube rows in either an in-line, staggered or partially staggered arrangement. For this thesis, the economiser is assumed to be in a perfectly in-line arrangement, as seen in Fig. 2.6. The economiser is then discretized into a number of elements, as seen in Fig. 2.6. The number of elements represents the number of parallel tubes. For each of the discretized parallel tube rows in the economiser, the differential conservation of mass, energy and momentum is applied, seen in Eqs. 2.53-2.55. Since the water is heated dynamically and allowed to boil, the three conservation equations are applied to each element. This ensures that if boiling occurs in the economiser, the fluid is pushed to the steam drum. This is also what happens in practice.

$$\frac{dM_{eco,i}}{dt} = \dot{m}_{eco,i+1} - \dot{m}_{eco,i} \quad (2.53)$$

$$\frac{dH_{eco,i}}{dt} = \dot{m}_{eco,i+1} h_{eco,i+1} - \dot{m}_{eco,i} h_{eco,i} + \dot{Q}_{f,i} \quad (2.54)$$

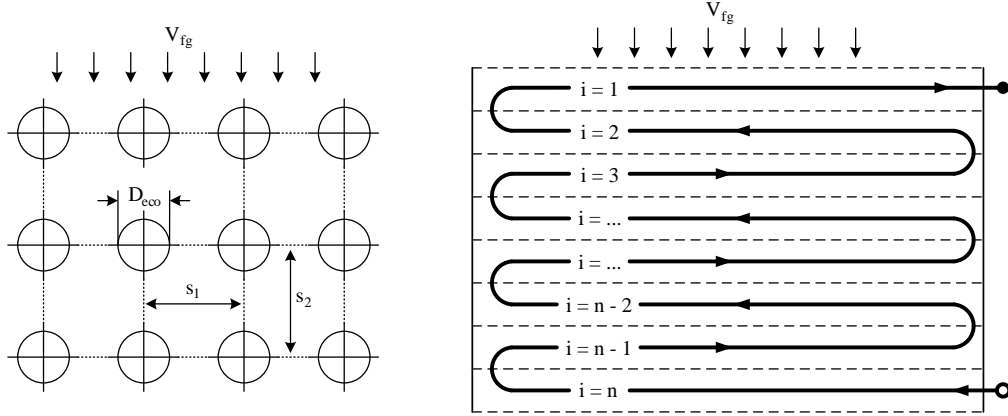


Figure 2.6: Economiser in an in-line arrangement with cross-flow heat exchange.

$$\frac{d\bar{v}_{eco,i}}{dt} = \frac{P_{eco,i+1} - P_{eco,i} - \Delta P_{loss,i}}{L_{eco,i} \cdot \bar{\rho}_{eco,i}} + \bar{v}_{eco,i} \frac{v_{eco,i+1} - v_{eco,i}}{L_{eco,i}} \quad (2.55)$$

The tube wall is modelled as described in section 2.5. The heat transferred from the flue gas to the tube wall is calculated as described in VDI Heat Atlas Appendix G7 [10]. A local Nusselt number is calculated for each row of tubes and the arrangement of the tubes is taken into account. The Nusselt number for each row is seen in Eq. 2.56.

$$Nu_{i,bundle} = f_A \cdot Nu_{l,0} \quad (2.56)$$

Where f_A is the tube arrangement factor and $Nu_{l,0}$ is the averaged Nusselt number for tubes in cross-flow. The tube arrangement factor takes the arrangement of the tubes into consideration. In this thesis it is assumed that the tubes are arranged in an in-line arrangement, as seen in Fig. 2.6. The tube arrangement factor for an in-line arrangement is given by Eq. 2.57.

$$f_{A,in-line} = 1 + \frac{0.7(b/a - 0.3)}{\psi^{1.5}(b/a + 0.3)^2} \quad (2.57)$$

The tube arrangement factor depends on the transverse pitch factor $a = s_1/d_0$ and the longitudinal pitch ratio $b = s_2/d_0$. The void fraction, ψ , describes the free space that the flue gas can travel through. If the tubes were arranged in a staggered or partly staggered arrangement, the correction factor would be different.

Since the temperature of the flue gas in this section is significantly lower, the thermal radiation is neglected and heat is only transferred through convection.

2.4.3 Superheaters

The saturated steam that leaves the steam drum is superheated in the superheaters. The superheater is a cross-flow heat exchanger as the economisers in section 2.4.2. It is also assumed that the superheaters are arranged in an in-line configuration, and the heat transferred from the flue gas is calculated using the same methodology as for the economisers. Since the superheated steam is not the scope of this study, the superheater is only modelled using conservation of energy. By only accounting for the heat transferred to the steam, the superheaters primary task is to lower the flue gas temperature before the flue gas reaches the economisers. During a warm start-up procedure, it is assumed that the tubes are filled with saturated steam. The amount of heat transferred to the steam is therefore low since the temperature of the flue gas is not considerably larger than the steam.

The conservation of energy applied to the discretized superheater rows are seen in Eqs. 2.58 and 2.59. The conservation of energy is applied to both the fluid and to the wall.

$$\frac{dH_{SH}}{dt} = \dot{m}_s(h_{i+1} - h_i) + \dot{Q}_{w \rightarrow f} \quad (2.58)$$

$$\frac{dT_{W,SH}}{dt} = \frac{\dot{Q}_{fg \rightarrow w} - \dot{Q}_{w \rightarrow f}}{M_w \cdot c_{p,w}} \quad (2.59)$$

2.5 Modelling of Tube Wall

The tube wall is modelled in one dimension and the main purpose of the tube wall is to act as a thermal resistance between the flue gas and the water and also to take into account the thermal inertia of the metal. The tube wall is modelled using only conservation of energy since no mass or momentum can be stored in the metal. The governing equation for the tube wall is seen in Eq. 2.60 and an overview of the tube wall is seen in Fig. 2.7. It is also seen in Fig. 2.7 that the heat transfer due to conduction in the steel is neglected. The tube wall is therefore assumed infinitely thin, which is a fair assumption since the temperature on the outside of the wall would only be slightly higher than on the inside.

$$\frac{dT_{w,i}}{dt} = \frac{\dot{Q}_{fg \rightarrow w,i} - \dot{Q}_{f,i}}{M_w \cdot c_{p,w}} \quad (2.60)$$

The heat transfer from the flue gas to the wall is described in section 2.2 and the heat transfer from the wall to the fluid is described in section 2.4.

The thermal properties of steel can either be assumed constant or be a function of temperature. For this thesis, the properties of steel are described as a function of temperature. It is assumed that the furnace tubes made of 15Mo3 steel. The

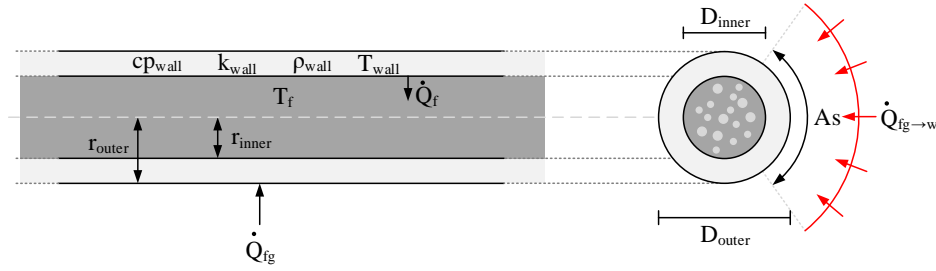


Figure 2.7: tube wall model including the dimensions and flow of energy in each tube segment.

thermal properties for 15Mo3 are given by the linear expressions seen in Eqs. 2.61 - 2.63 [18]. The density of 15Mo3 is simply assumed constant.

$$c_{p,w} = 0.1992 \cdot T_w + 457.24 \quad \left[\frac{\text{J}}{\text{kg} \cdot \text{K}} \right] \quad (2.61)$$

$$k_w = -0.0212 \cdot T_w + 48.992 \quad \left[\frac{\text{W}}{\text{m} \cdot \text{K}} \right] \quad (2.62)$$

$$\rho_w = 7850 \quad \left[\frac{\text{kg}}{\text{m}^3} \right] \quad (2.63)$$

2.6 Dynamic Instabilities

When simulating the phase transition of a fluid, instabilities are often experienced. This is both the case for steady-state and dynamic simulations. Instabilities are experienced when a system is 'swinging' between two feasible solutions, causing the system to never settle to a stable solution. The instabilities are seen both when a fluid is boiling and condensing. In this work where the fluid is boiling, the fluid goes from a high density to a low density in a very short time span making the system of equations very stiff.

The instabilities experienced are classified as steady-state instabilities and dynamic instabilities. Both classes of instabilities require that a two-phase flow is present. In this work, where the system is modelled dynamically, only the dynamic instabilities are described. Information concerning steady-state instabilities can be found in [14].

A flow is subject to dynamic instabilities when there is sufficient interaction and delayed feedback between the inertia of the flow and the compressible volume in front of the fluid [14]. According to Kakac and Bon [14], dynamic instabilities can be classified as:

1. Density wave oscillations
2. Pressure-drop oscillations
3. Acoustic oscillations
4. Thermal oscillations

For this work, the density wave oscillations were observed every time the fluid transitions into the two-phase region. As the pressure increases in the system, the oscillations become less dominating. At low pressures, the oscillating behaviour is observed. Density wave oscillations are described in the following section and the impact of the oscillations are also described.

2.6.1 Pressure-Drop Oscillations

When a phase transition occurs, a compressible volume is developed. The gas produced expands, causing the velocity to increase drastically in the system. The increased velocity causes a large pressure gradient, forcing the velocity of the system to decrease again. This causes the system to settle back to the previous state, where a phase transition once again occurs. The compressible volume developed introduces a time-lag in the system, which causes the system to become unstable. The pressure-drop oscillations are closely related to DWOs. Pressure-drop oscillations can only occur if there is a compressible volume in the system [14]. Since the water/steam mixture is modelled using a homogeneous approach, there is not a compressible volume present alone in the system. The fluid is always a homogeneous mixture, and the pressure-drop oscillations are not important for this thesis.

2.6.2 Acoustic Oscillations

The acoustic oscillations are caused by the resonance of the pressure wave experienced when a phase transition is experienced. These oscillations occur at high frequencies (10-100 Hz), since they are related to the time it takes the pressure wave to propagate through the system [14]. Since the pressure waves are propagating through a mixture of water and steam, the wave propagates fast, causing the oscillations to occur at the speed of sound in the medium. These oscillations do not have much importance for this thesis since the time resolution is not sufficiently small to resolve these oscillations.

2.6.3 Thermal Oscillations

Thermal oscillations are experienced when the flow experiences varying heat transfer coefficients. The varying heat transfer coefficient results in large magnitude temperature differences in the solids [14]. The large temperature difference in the solids causes the boiling flow to transition between different boiling regimes

(see App. B). At different boiling regimes, the fluid will have different velocities, resulting in pressure and velocity oscillations. Since the fluid is modelled using a homogeneous mixture model, the boiling regimes are not taken into consideration, and the thermal oscillations are not experienced in the model developed.

2.6.4 Density Wave Oscillations

When a fluid is starting to boil in the system, the density goes from a high value to a low value. In this work where the working fluid is water, the density wave oscillations are mostly experienced at low pressures. This is due to the fact that the density drops from a value of approximately 1000 kg/m^3 to 50 kg/m^3 , as seen in Fig. 2.8. As the pressure increases, the gradient of the density becomes less steep,

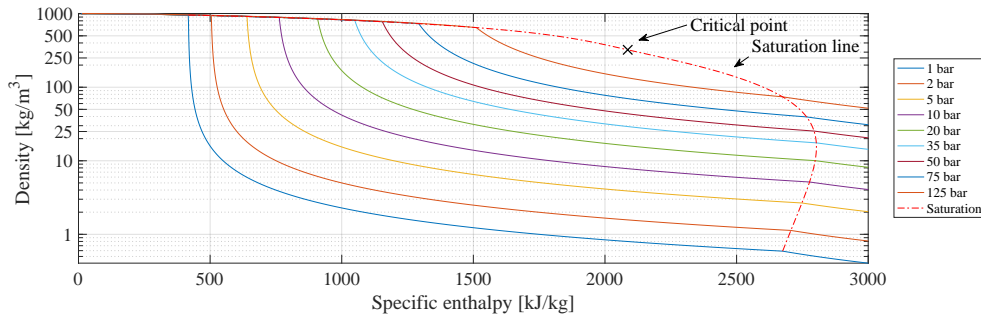


Figure 2.8: Density isobars as a function of specific enthalpy.

as seen in Fig. 2.8. When the fluid enters the two-phase region, the density drops drastically resulting in an increased velocity due to the lower density. The larger velocity causes the pressure gradient to increase, resulting in a decreased inlet flow of the high-density fluid. The fluid swings between these two states where the two-phase mixture have a large velocity, causing the pressure gradient to increase and thereby slowing down the fluid. This is seen throughout the simulations since the velocity oscillates due to the pressure inside each element.

The density wave oscillations are caused by the first derivative discontinuity according to Johansen et al. [13]. To increase the stability of the numerical solver, Johansen et al. propose to dampen the oscillations by introducing either a smooth transition function or by introducing an artificial damping coefficient. In this work neither have been introduced, since a sufficiently small time step is able to resolve the oscillations. The cost of the sufficiently small time step is an increased computational time, which has been accepted for this thesis.

A typical DWO is seen in Fig. 2.9, where the velocity of the fluid increases rapidly when the fluid transitions into the two-phase region. As the density decreases, the velocity increases and thereby the pressure gradient increases. This

causes the system to find another feasible solution, causing the velocity to decrease and the density to increase. If the system was operating in steady-state, the system would swing between these two solutions and have trouble settling to a single solution. In this example, the pressure is increased over time, forcing the system to find a single feasible solution.

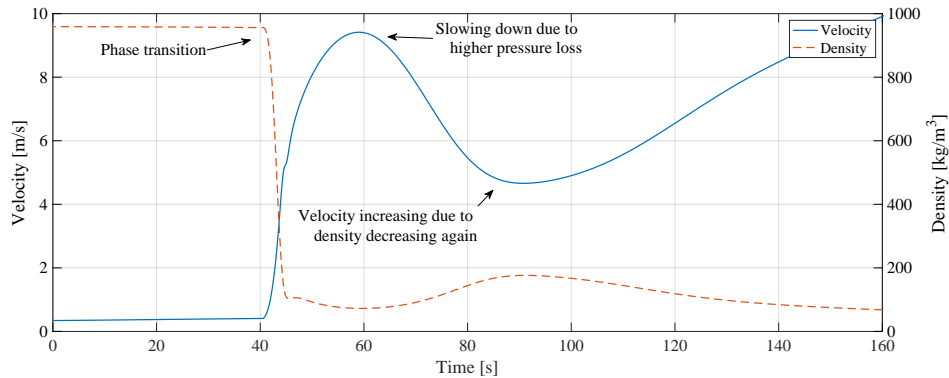


Figure 2.9: Typical density wave oscillations

When the model was initially developed, the density wave oscillations caused a lot of instability in the system which often caused the program to crash, but when the evaporator circulation loop was coupled with the steam drum and the pressure was allowed to increase over time, the problem became less dominating. The coupling caused the pressure oscillations due to DWOs to become less dominating and the system would thereby stabilise itself since the phase transitions are only observed once for each of the discretized elements.

The density wave oscillations are an important parameter when modelling the dynamic phase transition of water. When the fluid starts to boil and the density decreases, the rapid expansion causes the liquid to be displaced. The liquid is then 'pushed' to the above elements and finally to the steam drum. This rapid expansion of water is the cause of rapid swelling inside the steam drum, and it is therefore important to resolve the DWOs.

2.7 Chapter Summary

A model to describe the dynamic behaviour of a steam boiler with natural circulation is developed. The model is summarised in Fig. 2.10. At every time step, the model developed is solved using MATLAB's built-in solver ODE15s. The ODE15s solver is a stiff solver with a 1st to 5th order accuracy [19]. The solver is able to detect rapid changes within the system and adjust the time step. To resolve the steep gradients of the phase transition, the solver is limited to a small time step, since the steam table used is not able to calculate negative densities, enthalpies, etc. which is mathematically possible when using large time steps.

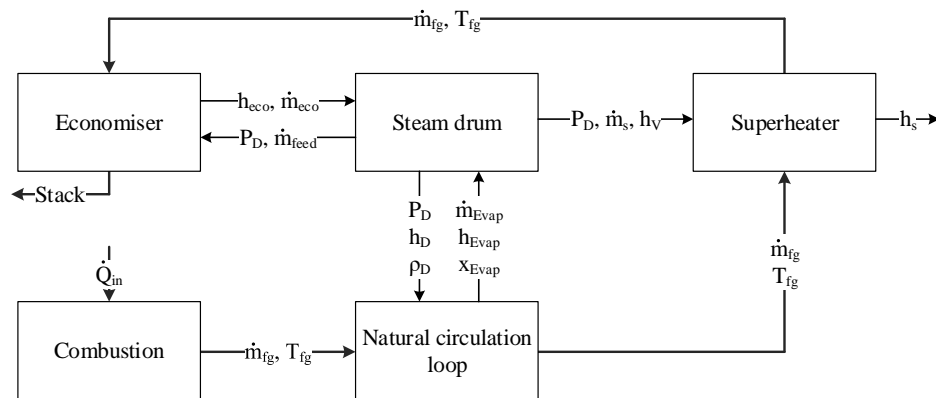


Figure 2.10: Model in- and outputs for the different groups of components.

Chapter 3

Results and Discussion

In this chapter, the results of the simulations are presented following a discussion of the obtained results. An initialisation strategy is presented before the results of the simulations.

3.1 Initialisation

In order to simulate the warm start-up procedure of a plant, an initialisation strategy is presented. The plant is simulated using the assumption that boiling occurs in the economiser during purging. During purging, there is a large flow of flue gas through the boiler and the flue gas temperature is slightly higher than the water walls. It is assumed that the temperature of the flue gas is 150 K higher than the lowest part of the evaporator. This assumption is reasonable since the highest temperatures are located in the lowest part of the boiler. A large thermal inertia is present in the lowest part of the boiler since the grate and refractory are placed in this part of the boiler. The grate consists of several tons of steel and the refractory also consist of several tons. The flue gas entering the boiler is therefore heated in the lowest part of the boiler, and the assumption that the flue gas is heated to 150 K above the saturation temperature is acceptable. The hot flue gas stored in the lowest part of the boiler is 'pushed' through the rest of the boiler plant.

To ensure that water starts to circulate in the correct direction, the water in the system is subcooled by a few degrees below the saturation temperature. The subcooling of water is introduced, since the fast expansion of water when boiling occurs resulted in water circulating backwards in the evaporation loop. The subcooled water solved this problem since the water will circulate with a low velocity before boiling occurs. The entire plant is assumed to be in thermal equilibrium at $t = 0$ s, meaning the flue gas temperature occupying the volume inside the boiler is the same temperature as the water walls.

It is assumed that the steam drum is filled with water to obtain a certain water

level, and the remaining free volume is occupied with saturated steam.

To analyse the impact of swelling in the steam drum during a warm start-up procedure, the feedwater controller is switched off during the simulation. This is done, to ensure that the water level analysed is only a function of the fast expansion of water in the evaporator and economiser. The simulations are carried out for an initial steam drum pressure in the range of 5 bar_a to 20 bar_a.

The initialisation strategy is summarised in Tab. 3.1 with the initial values used as in input to the model described in Chapter 2.

Table 3.1: Initial input values to the simulation of the warm start-up procedure. * See Fig. 2.5 for discretization.

| Description | Symbol | Initial value | Unit |
|-----------------------------|------------------|----------------------------|------------------|
| Drum water level | L_L | -80 | mm |
| Feedwater controller gain | k_p | 0 | - |
| Flue gas flow | \dot{m}_{fg} | 20 | kg/s |
| Flue gas temperature inlet | $T_{fg,in}$ | $T_{sat}(P_{n+1})^* + 150$ | °C |
| Fluid temperature | T_f | $T_{sat}(P_i) - 2.5$ | °C |
| Fluid velocity | v_f | 0 | m/s |
| Initial steam drum pressure | P_D | [5, 20] | bar _a |
| Maximum pressure | P_{max} | 92 | bar _a |
| Temperature gradient | $dT_D/dt _{max}$ | 2.5 | K/min |

3.2 Simulation Results

The model is started using the initialisation strategy, described in section 3.1, and is simulated until the impact of the phase transition is no longer dominating. This means that the simulation is stopped after approximately 90-110 s. At this point, the water level is decreasing, which is seen in Fig. 3.8. The maximum impact of the boiling in both the evaporator and economiser has been observed for the heat input, and the simulation is therefore stopped.

The initial pressure of the entire system is determined from the initial steam drum pressure. When the entire system is at rest, the pressure in the riser tubes is larger than the steam drum pressure due to the geodetic pressure contribution. The simulations are carried out for initial steam drum pressure of 5, 7.5, 10, 14, 15 and 20 bar_a. The following results are presented for an initial steam drum pressure of 14 bar_a.

3.2.1 Mass Fraction of Steam

When the plant is initially started, the slightly hotter flue gas is purged through the boiler, driving the circulation of water in the evaporator. The fluid needs to be heated from subcooled to saturation before boiling occurs, and during this time, a stable circulation is established. While the circulation of water is started, the steam mass fraction remains constant, as seen in Fig. 3.1. During this time a small amount of water circulates inside the tubes, resulting in an almost constant steam mass fraction. When the fluid starts to circulate, the subcooled water approaches saturation. Boiling occurs in the evaporator after approximately 80 seconds of simulation time, also seen in Fig. 3.1.

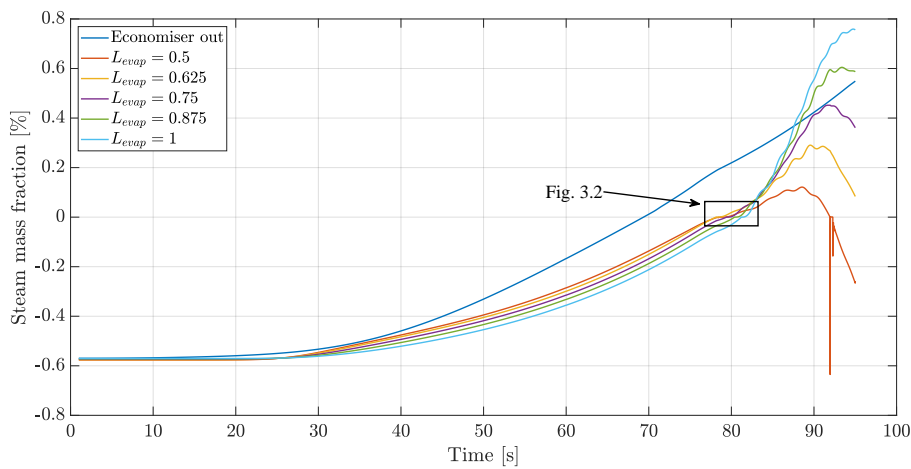


Figure 3.1: Steam mass fraction as a function of time for the relative pipe length in the evaporator at the initial steam drum pressure of 14 bar_a.

The top row of tubes in the economiser reaches saturation before the evaporator, as seen in Fig. 3.1. This is due to a large amount of flue gas being purged through the boiler, resulting in a relatively high flue gas temperature reaching the economisers. Furthermore, the pressure of the economiser is lower than the evaporator, resulting in the economiser starting to boil first. Boiling is observed in the economiser after $t \approx 70$ s, and the steam mass fraction increases almost linearly after the phase transition has occurred.

The water in the evaporator starts to boil in the middle of the evaporator. This is observed for all the simulated pressures. The water starts to boil in the middle of the evaporator due to the low circulation of water.

A close-up view of the evaporator starting to boil is seen in Fig. 3.2. Boiling is first observed in the evaporator at a relative length of $L_{evap} = 0.625$. After 1 second of additional simulation time, the element located below, at a relative length

of $L_{evap} = 0.5$, starts to boil. The steam produced in the middle elements moves into the above-located elements in the evaporator, resulting in the remaining elements of the evaporator boiling within a short period of time. From the first phase transition is observed, it takes 3 seconds for the top half of the evaporator to start boiling. This means that 5 phase transitions have been observed within 3 seconds, which results in a significantly increased mass flow leaving the evaporator, also seen in Fig. 3.3.

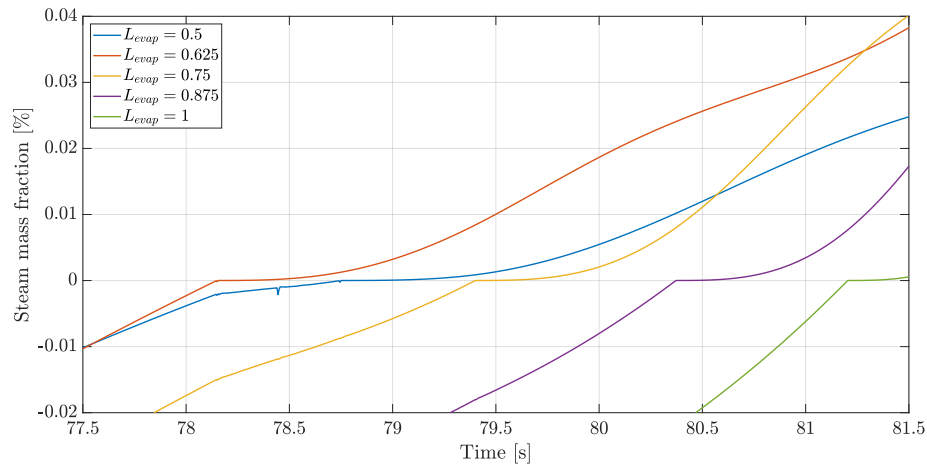


Figure 3.2: A close-up view of the steam mass fraction as function of time for the relative pipe lengths. First phase transition is observed for the relative pipe length of 0.625. The results are shown for an initial steam drum pressure of 14 bar_a.

3.2.2 Mass Flow of Water and Steam

During the warm start-up procedure, the subcooled water inside the riser tubes are initially at rest, and when heat is applied, the water starts to circulate, as seen in Fig. 3.3. The mass flow is normalised to highlight the increased mass flow after boiling occurs, and therefore the mass flow, seen in Fig. 3.3, is normalised using the mass flow just before boiling is experienced as a reference. A normalised mass flow of 1 is observed at the phase transition in the first boiling element. By doing this normalisation of the mass flow, the effect of the phase transition is easily observed.

The mass flow leaving the discretized elements are increased until saturation is obtained. When boiling is observed, as described in section 3.2.1, the mass flow increases significantly. The water in the discretized elements expands rapidly when steam is being formed during the phase transition. This results in an increased flow in the element due to the steam displacing the water in the element. Therefore the mass flow leaving the discretized element is increased significantly, eventually

resulting in a large mass of water being 'pushed' to the steam drum. This results in the flow being increased by 560 % compared to the single-phase flow.

The pressure inside the steam drum is also seen in Fig. 3.3. During the start-up, the pressure is only increased slightly until boiling is experienced. During boiling more steam is produced than can be stored in the steam drum, causing the pressure to be increased, controlled by the maximum allowable pressure gradient. After the phase transition has occurred, steam also leaves the steam drum.

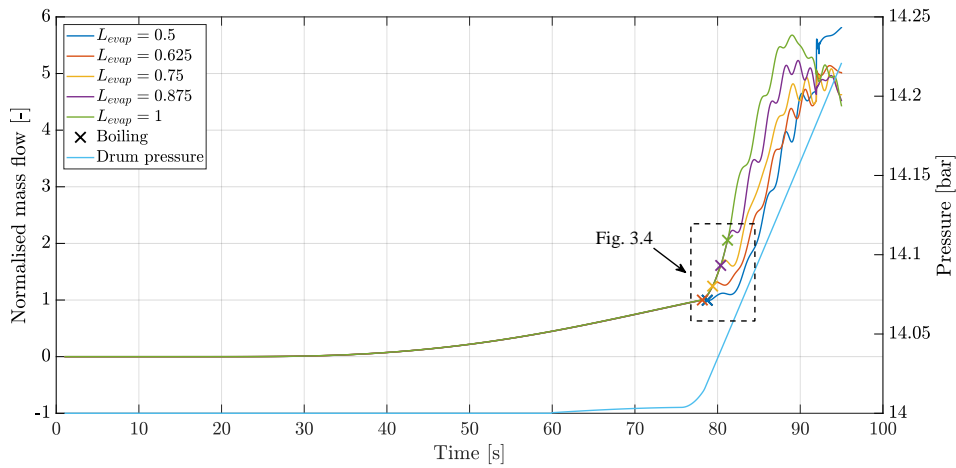


Figure 3.3: Normalised mass flow of the evaporator as a function of simulation time for the relative pipe lengths. The mass flow is normalised using the mass flow just before boiling in the first element. Phase transitions in the discretized pipe lengths are marked with cross.

A close-up of the mass flow in the discretized elements is seen in Fig. 3.4. Whenever a phase transition is observed, the mass flow is increased in the boiling element and the above-located elements. The mass flow is also decreased in the below-located elements during boiling. This same tendency is observed every time boiling occurs. The largest mass flow is seen in the top element due to the mass from the lower located elements being 'pushed' to this element. Approximately 5 seconds after the first phase transition is observed, the mass flow leaving the evaporator is increased by approximately 400 %.

The economiser starts to boil before the evaporator, as seen in Fig. 3.1. While the water in the economiser is subcooled, $t < 70$ s, the mass leaving the economiser is almost negligible ($\dot{m}_{eco,out} \approx 0$). As soon as boiling is experienced in the economiser, the mass flow leaving the economiser increases significantly. As the phase transition is observed, a mass flow of 35 kg/s is experienced, as seen in Fig. 3.5. The mass flow increases from 0 kg/s to 35 kg/s in a very short period of time. The rapid mass flow is due to the rapid formation of steam displacing the water in

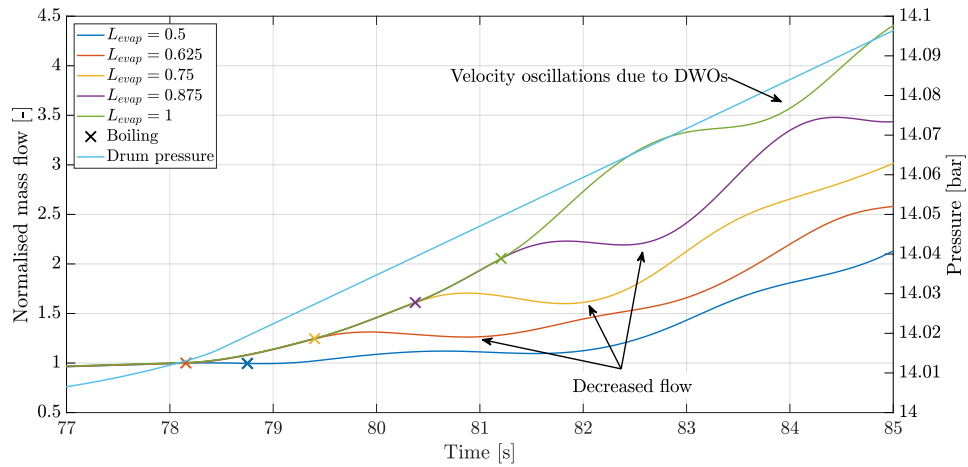


Figure 3.4: A close-up view of the normalised mass flows in the discretized evaporator elements during boiling. The close-up view is also marked on Fig. 3.3.

the tube row. After the maximum flow leaving the economiser, the flow starts to oscillate and this is due to the density wave oscillations experienced at the phase transition. It is seen that the oscillations become smaller and trends to a stable flow, but the simulation is stopped before the flow becomes stable. Boiling in the economiser is only experienced in the top row tubes, and if boiling were to occur in the second top row, oscillations would be experienced again.

The rate of accumulation of water and steam in the steam drum is seen in Fig. 3.6. The rate of accumulation is the sum of water and steam entering and leaving the steam drum. The figure starts from 60 s, since the rate of accumulation of water and steam before this point is approximately 0, due to the low circulation of water. When boiling occurs in the economiser, the mass gradient increases, and the DWOs are observed here. When boiling occurs in the evaporator, the rate of accumulation for water increases, and the rate of accumulation for steam decreases simultaneously. After approximately 10 seconds the gradient decreases again, and water starts to leave the steam drum. This is due to an increasing density in the elements. The density increases in the elements, since the circulation of water forces more water to enter the lowest elements in the evaporator tubes, also seen in Fig. 3.7. A lower temperature is present in the steam drum, since a large amount of water is stored here, and this forces the density of the elements to increase again. The lowest elements are thereby 're-filled' with water after the steam has displaced it.

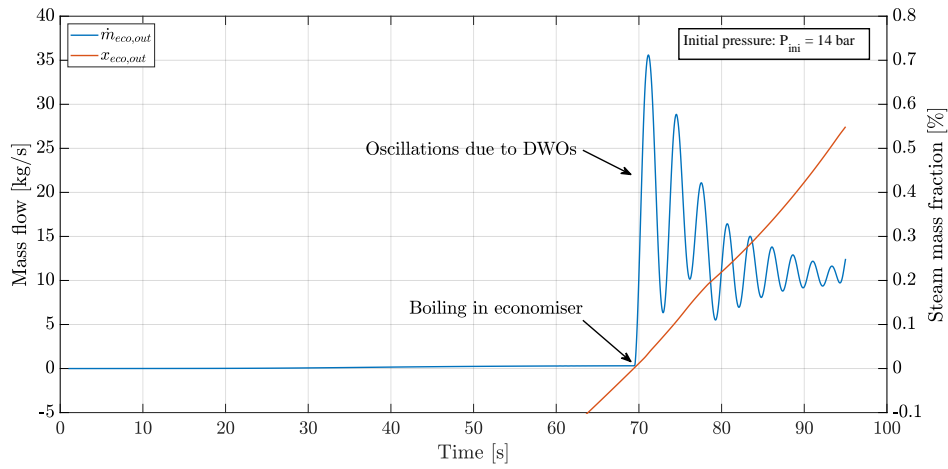


Figure 3.5: Mass flow and steam mass fraction at the outlet of the evaporator. The results are shown for a starting drum pressure of 14 bar_a. The mass flow is oscillating due to the DWOs occurring at the phase transition.

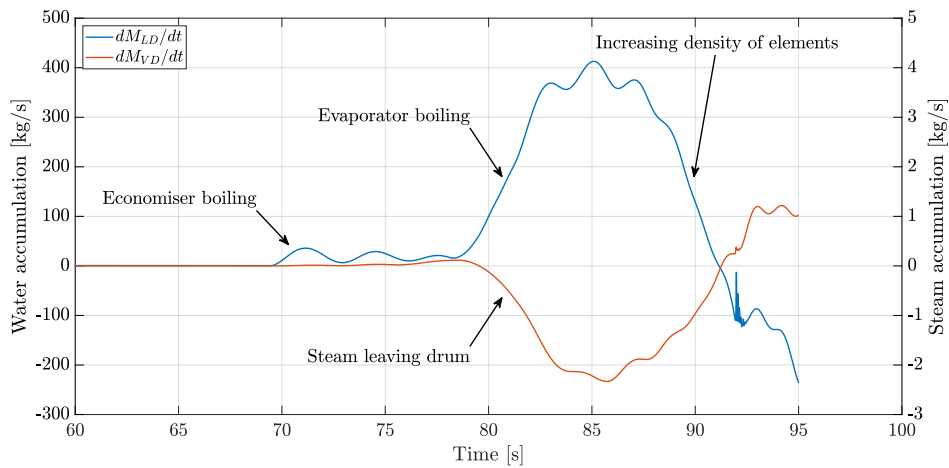


Figure 3.6: Total mass of water and steam in the steam drum. The sum of the mass flow before 60 s is close to 0, due to the low circulation.

The 're-filling' of the elements are also seen when analysing the density changes in the evaporator and economiser. The density of the discretized elements and the outlet of economiser is seen in Fig. 3.7. The DWOs are observed for the all discretized elements experiencing a phase transition. The density oscillates for both the economiser and evaporator elements. As seen in Fig. 3.6, the water starts to leave the steam drum after approximately 87 seconds, and it is observed in Fig. 3.7 that the density of the lowest elements starts to increase at this time. It is seen that element located at $L_{evap} = 0.50$ enters the two-phase regime after $t \approx 80$ s, and after 10 s the fluid is back to the single-phase regime. The same tendency is seen for the elements at $L_{evap} = 0.625$ and $L_{evap} = 0.75$, but the simulations is stopped before the elements enters the single-phase regime.

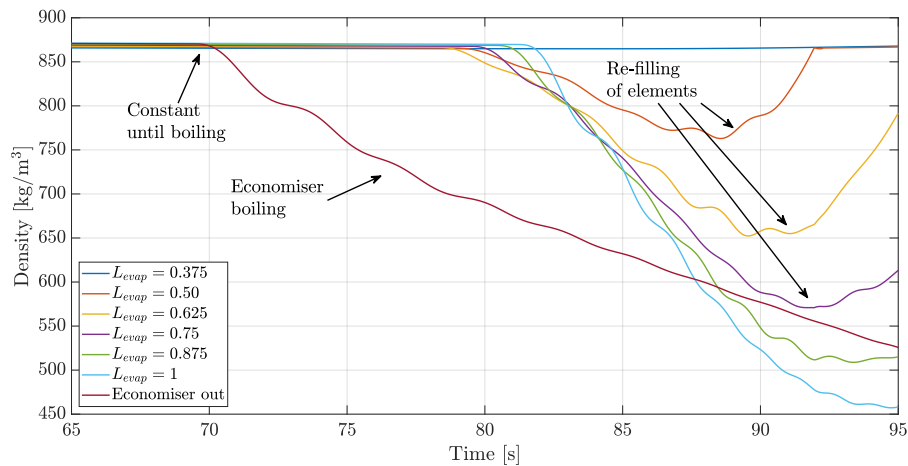


Figure 3.7: Density of the economiser and the discretized evaporator elements. The density for $t < 65$ s is almost constant, which is why this section is cut off. The results are shown for an initial steam drum pressure of 14 bar_a.

3.2.3 Water Level of Steam Drum

The water levels inside the steam drum are seen in Fig. 3.8 for the alternating initial drum pressures. The water level is displayed as a reference to the desired set level. The dashed lines in Fig. 3.8 indicate the water level in the steam drum if only the evaporator model was included in the simulation. The full line is for both the economiser and evaporator model, and it is clearly seen that the boiling in the economiser causes the water level in the steam drum to increase. It is clearly seen that before boiling occurs, $t < 70$ s, the water level inside the steam drum is almost constant. The water in the entire system is subcooled by 2.5 K, and the density of water is almost constant until boiling is experienced. If the simulation

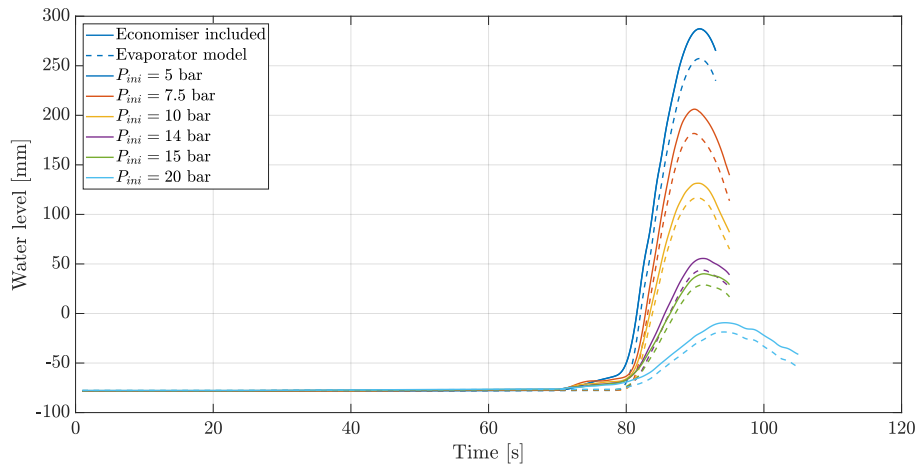


Figure 3.8: Steam drum water level at different initial steam drum pressures. The water level is a reference to the desired set level, denoted by a water level of 0. The dashed lines indicate the water level if only the evaporator model was included.

was performed for a cold start-up, the water level would increase more, since the density of the subcooled water changes more during a cold start-up.

When boiling occurs, at $t > 70$ s, the water level rises due to the mass flow leaving the economiser. When boiling in the evaporator is experienced, the water level in the steam drum increases significantly, as seen in Fig. 3.8. The water level increases significantly since a large amount of water is stored in the water walls. Due to the large amount stored in the water walls, the water is 'pushed' to the steam drum.

The same tendency is seen for all the simulated initial pressures, where the water level increases to a maximum and then decreases, as steam starts to leave the steam drum and the lowest elements are 're-filled' with water. The feedwater controller is switched off during these simulations, and the water level decreases in all the simulations. If the controller were active, the desired water would eventually be achieved.

It is clearly seen in Fig. 3.8 that the water level increases as a function of the initial steam drum pressure. Since the tendency of the water level curves is similar for all the simulated initial steam drum pressures, a correlation between the maximum water level in the steam drum and initial steam drum pressure is made. The maximum water level is represented as the relative water volume in the steam drum, which is essentially the percentage of water occupying the volume of the steam drum. The relative volume of water is chosen instead of the water level, since the volume of the steam does not scale linearly with the water level, due to the complex geometry of the steam drum. The relative water volume in the steam

drum as a function of the relative drum pressure, seen in Fig. 3.9, gives a clear understanding of how the steam drum is filled with alternating starting pressures.

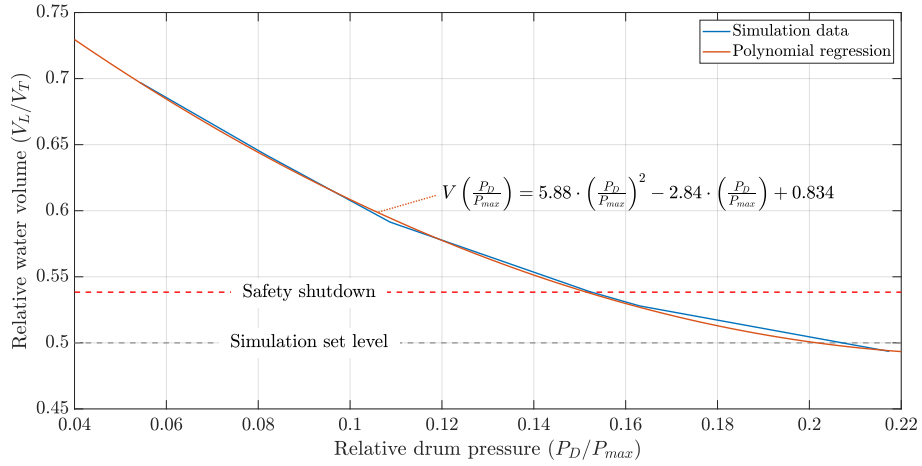


Figure 3.9: Relative water level as function of relative initial steam drum pressure. The desired relative water volume is chosen as the radius of the steam drum, and the safety shutdown value is given as 55 mm above the desired set level.

As seen in Fig. 3.9, the volume of water in the steam drum is larger than the desired volume for relative pressures smaller than $P_D/P_{max} < 0.2$, and this is due to the large volumetric expansion of water below this pressure. A typical shutdown water level is also seen on Fig. 3.9, and here the shutdown water level value is marked as 55 mm above the set level. If the water level were to exceed this value, the plant shuts off for safety reasons, and the steam drum has to be drained. As seen in Fig. 3.9, the water level exceeds this value for relative starting pressure of $P_D/P_{max} < 0.15$.

A second order polynomial regression is made for the observed data points, and the regression has a good fit within the simulated pressure range. The second order polynomial is seen in Eq. 3.1 and is valid for initial steam drum pressures in the range of [5, 20] bar_a. The polynomial regression is only valid for the simulated initial pressures, as seen in Fig. 3.9.

$$V\left(\frac{P_D}{P_{max}}\right) = 0.588 \cdot \left(\frac{P_D}{P_{max}}\right)^2 - 2.84 \cdot \left(\frac{P_D}{P_{max}}\right) + 0.834 \quad (3.1)$$

3.3 High Water Levels in Practice

When water starts to boil in the economiser, as shown in the previous section, the water level rises, and it would be convenient to measure this increased flow to the steam drum. In practice, the boiling flow leaving the economiser is not usually measured, since the flow measuring equipment is located between the feedwater pump and the economiser, as seen in Fig. 3.10.

The flowmeter is located here, since the temperature of the water is low, and single-phase flow is always obtained at this point. Measuring the flow between the economiser and steam drum is more difficult since the temperature of the water is much higher ($T_w > 300^\circ\text{C}$). Steam can also be present in the flow when boiling in the economiser is experienced, making it even more complex to measure. Installing an additional flowmeter between the economiser and steam drum allows to measure the phenomena where boiling occurs in the steam drum. This also allows for measuring the phenomena where a steam pocket collapses in the economiser. During a warm start-up procedure, it is sometimes experienced, that steam is present in the economiser, and when cold air passes through the economiser, the steam condensate, essentially, 'sucking' the water from the steam drum to the economiser. During this phenomena, the boiler is shut down for safety reasons due to low water levels. The measuring equipment could potentially be retrofitted to existing plants as clamp-on flowmeters, e.g. ultrasonic flowmeters.

The high water levels obtained in the simulations are a function of the initial starting pressure, but in practice, a solution has to be found when starting at a lower pressure. When boiling is experienced in both the economiser and the evaporator, the steam produced displaces the water in the elements. To maintain a certain water level, water is in practice discharged from the steam drum using a *blowdown* valve. The water is blown from the steam drum to a secondary tank, but the blowdown valve can only handle a certain amount of water. The blowdown of water is costly if warm start-up procedures have to be performed on a regular basis and to avoid wasting too much water, it would be preferable to start from a pressure where the maximum allowable water level is not exceeded. To ensure that the pressure does not decrease below the desired minimum pressure, hatches can be installed for at the air in-take and at the flue gas outlet. By installing hatches,

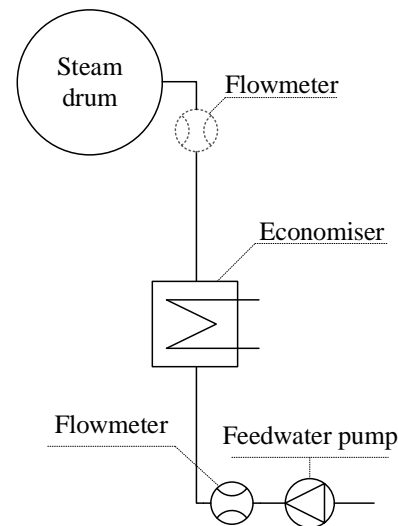


Figure 3.10: Installation of an additional flowmeter allows for measurements of boiling in the economiser.

the cold air entering the furnace is limited to a minimum, and the cooling of the plant is reduced.

Alternatively, a free volume can be obtained in the system by draining the economiser. The free volume serves as a buffer, where the displaced water can be stored when boiling in the economiser is experienced. By doing this, a large amount of unwanted water never reaches the steam drum during the start-up procedure. The issue with draining the economiser is that the drained water is valuable, especially if the warm start-up procedure has to be performed on a regular basis. This solution can be used if start-ups are performed for low pressures.

Chapter 4

Conclusion

In this thesis, a mathematical model describing the dynamic behaviour of a natural circulation biomass boiler is developed. The mathematical model consists of a system of differential equations coupled with a system of non-linear algebraic equations. The system of equations is solved using MATLAB's ODE15s solver for stiff systems. The model developed describes the transient evaporation of water during a warm start-up procedure for a large biomass boiler consisting of a steam drum, an evaporator, superheaters and economisers. During a warm start-up, the water is close to saturation, and a small amount of heat added results in boiling. The economiser and evaporator start to boil during purging, and the steam produced displaces the water in the tubes, resulting in a higher water level in the steam drum.

The simulations are carried out for pressures of 5, 7.5, 10, 14, 15 and 20 bar_a, resulting in alternating maximum water levels in the steam drum. For the lowest simulated pressure a water level of +280 mm above the set level is obtained, and for the highest pressure simulated, a water level of -10 mm is obtained. A correlation between the relative volume of water in the steam drum and the relative initial starting pressure is developed. Depending on how much the steam drum is allowed to be filled with water, the initial starting pressure can be found from the expression. If a maximum water level of +50 mm were to be obtained, an initial steam drum pressure of 14.2 bar_a should be chosen as the minimum starting pressure if no draining has to be conducted during start-up. If higher allowable water levels are allowed, lower starting pressure can be allowed. If the plant is started at lower pressures, the water in the system has to be drained to ensure a safe start-up.

Boiling in the economiser is observed for all simulated pressures. When boiling is experienced in the economiser, the steam produced displaces water, resulting in a large mass flow leaving the economiser. In the evaporator, boiling is first observed in the middle of the evaporator for all simulated pressures. Since the circulation of water is low during the warm start-up procedure, the water starts to boil in the

middle elements before a sufficiently large circulation is established. When boiling is observed, a significantly increased mass flow leaving the evaporator is seen. The mass flow is increased by approximately 560 % compared to the single-phase mass flow. The significantly increased mass flow results in a rapid accumulation of water in the steam drum. Over a short period of time, the top half of the evaporator is boiling, causing the significantly increased mass flow. Within the simulated time ($t < 100$ s) the water starts to leave the steam drum, to 're-fill' the lowest located elements with water, since the increased circulation of water forces subcooled water to enter the lowest located elements. The rate of accumulation of water is thereby negative after the rapid swelling inside the steam drum. This tendency is observed for all simulated pressures.

The knowledge gained in this project enlightens the boiling in both the evaporator and economiser during a warm start-up procedure. To limit high water levels in the steam drum, the minimum starting pressure for this specific system can be obtained using the correlation presented.

Chapter 5

Future Work

The complex geometry of the boiler is simplified to 300 parallel evaporator tubes and 20 rows of economiser tubes. All the evaporator tubes experience the same heat flux and are identical, which is not the case in practice. This is also the case for the economiser, where the entire row of tubes is subject to the same flue gas temperature, which is also not the case in practice. The heat applied to the front, back and sidewalls in the furnace are not identical since the flue gas moves at different velocities inside the furnace. A stream of hot air can be present from the combustion, causing more heat to be transferred to the front wall for example. By transferring more heat to the front wall, boiling would be experienced at an earlier stage compared to the remaining walls. By having boiling in one of the walls and not the three others could cause parallel boiling instability, where the pressure gradient is much larger in the boiling wall. This causes the system to become unstable, and this phenomenon could be interesting to analyse. The flue gas inside the furnace would be interesting to analyse, in order to simulate the heat transfer to the evaporator tubes, and a CFD simulation could be carried out to analyse the hot and cold zones inside the furnace.

The water/steam mixture is assumed homogeneous in this work, meaning that there is no slip between the two phases. This assumption could possibly be improved by modelling the two phases separately. By doing so, a void fraction of steam needs to be calculated, and the slip between the two phases can be taken into consideration. The advantage of modelling the two phases separately in the economiser and evaporator is that the water does not move at the same velocity as the steam. This could possibly result in a more realistic representation of the rapid swelling in the steam drum since the water would move slower than the steam. It is expected that the swelling would be slightly slower, but that the impact of the displaced water is the same.

Aalborg Energie Teknik A/S observes the rapid increases in water level during a warm start-up, but they do not measure the flow entering the steam drum.

It is therefore unknown if the mass entering the steam drum is coming from the economiser or the evaporator. It would be interesting to make experimental work, to observe the boiling flow entering the steam drum. This could be performed using the strategy described at the end of Chapter 3. Installing a flowmeter between the economiser and steam drum would allow measuring the boiling and condensation of water during a warm start-up. It would be interesting to analyse under what conditions boiling and condensation occurs in a plant, and if the phenomena only occur for the individual plant or it can be generalised for different plants.

Bibliography

- [1] Aalborg Energie Teknik A/S. *Tilbury Green Power photo*. 2017. URL: www.aet-biomass.com.
- [2] K. S. Bhambare, Sushanta K. Mitra, and U. N. Gaitonde. "Modeling of a Coal-Fired Natural Circulation Boiler". In: *Energy Resource Technology* 129 (2006), pp. 159–167. DOI: <https://doi.org/10.1115/1.2719209>.
- [3] Kasper Gram Bilde. *Dynamic Operation of Natural Circulation Evaporators during Cold Start-Up*. 9th semester project during internship at Aalborg Energie Teknik A/S. 2018.
- [4] Yunus A. Cengel. *Fundamentals of Thermal-Fluid Sciences*. McGraw-Hill, 2002. ISBN: 9780072458930.
- [5] Vijay Chatoorgoon. "SPORTS - A simple non-linear thermalhydraulic stability code". In: *Nuclear Engineering and Design* 93.1 (1986), pp. 51 –67. DOI: [https://doi.org/10.1016/0029-5493\(86\)90194-9](https://doi.org/10.1016/0029-5493(86)90194-9).
- [6] Xianbing Chen et al. "An experimental investigation of flow boiling instability in a natural circulation loop". In: *International Journal of Heat and Mass Transfer* 117 (2018), pp. 1125 –1134. DOI: <https://doi.org/10.1016/j.ijheatmasstransfer.2017.10.076>.
- [7] John G. Collier and John R Thome. *Convective Boiling and Condensation*. 3rd. Oxford University Press, 1994. ISBN: 0198562829.
- [8] Brian Elmegaard. *Simulation of Boiler Dynamics: Development, Evaluation and Application of a General Energy System Simulation Tool*. English. Department of Energy Engineering, 1999.
- [9] Energinet. *Hvor kommer strømmen fra?* Visited: 30-01-19. 2018. URL: <https://energinet.dk/El/Miljoedeklarationer/Hvor-kommer-stroemmen-fra>.
- [10] Volker Gnielinski. "G7 Heat Transfer in Cross-flow Around Single Rows of Tubes and Through Tube Bundles". In: *VDI Heat Atlas*. Berlin, Heidelberg: Springer Berlin Heidelberg, 2010, pp. 725–730. ISBN: 978-3-540-77877-6. DOI: [10.1007/978-3-540-77877-6_40](https://doi.org/10.1007/978-3-540-77877-6_40).

- [11] Ernst Hairer, Syvert Paul Nørsett, and Gerhard Wanner. *Solving Ordinary ,Differential Equations II. Stiff and Differential-Algebraic Problems*. Springer-Verlag, 2002. ISBN: 978-3-642-05220-0.
- [12] Bonnie J. McBride, Sanford Gordon, and Martin A. Reno. "Coefficients for calculating thermodynamic and transport properties of individual species". In: *NASA Technical Memorandum 4513* (1993).
- [13] Axel Vodder Ohrt Johansen et al. "Numerical study of evaporators in power plants for improved dynamic flexibility". English. PhD thesis. DTU Mechanical Engineering, 2013.
- [14] S. Kakac and B. Bon. "A Review of two-phase flow dynamic instabilities in tube boiling systems". In: *International Journal of Heat and Mass Transfer* 51.3 (2008), pp. 399–433. DOI: <https://doi.org/10.1016/j.ijheatmasstransfer.2007.09.026>.
- [15] Satish Kandlikar. "A General Correlation for Saturated Two-Phase Flow Boiling Heat Transfer Inside Horizontal and Vertical Tubes". In: *Journal of Heat Transfer-transactions of The ASME* 112 (Feb. 1990), pp. 219–228. DOI: 10.1115/1.2910348.
- [16] H. Kim and S. Choi. "A model on water level dynamics in natural circulation drum-type boilers". In: *International Communications in Heat and Mass Transfer* 32.6 (2005), pp. 786–796. DOI: <https://doi.org/10.1016/j.icheatmasstransfer.2004.10.010>.
- [17] Klaus Krüger, Rüdiger Franke, and Manfred Rode. "Optimization of boiler start-up using a nonlinear boiler model and hard constraints". In: *Energy* 29.12 (2004), pp. 2239–2251. DOI: <https://doi.org/10.1016/j.energy.2004.03.022>.
- [18] M. Woite GmbH. *Material No.: 1.5415*. Material properties of steel 15Mo3. Date visited: 30-01-19. 2012. URL: <http://www.woite-edelstahl.com/15415en.html>.
- [19] Mathworks. *Choose an ODE Solver*. Date visited: 20-11-2018. URL: <https://se.mathworks.com/help/matlab/math/choose-an-ode-solver.html>.
- [20] United Nations. *Sustainable Development Goals*. Visited: 30-01-19. 2015. URL: <https://www.un.org/sustainabledevelopment/sustainable-development-goals/>.
- [21] Michael Korsgaard Nielsen. *Danmark bliver kulbrit i 2030*. Visited: 30-01-19. 2017. URL: <https://www.berlingske.dk/virksomheder/danmark-bliver-kulbrit-i-2030>.

- [22] Almir Sedić, Stjepko Katulić, and Danijel Pavković. “Dynamic model of a natural water circulation boiler suitable for on-line monitoring of fossil/alternative fuel plants”. In: *Energy Conversion and Management* 87 (2014), pp. 1248–1260. DOI: <https://doi.org/10.1016/j.enconman.2014.06.059>.
- [23] Kim Sørensen. “Dynamic Boiler Performance: Modelling, simulating and optimizing boilers for dynamic operation”. PhD thesis. Institut for Energiteknik, Aalborg Universitet, 2004. ISBN: 87-89179-52-8.
- [24] P. U. Sunil, Jayesh Barve, and P.S.V. Nataraj. “Mathematical modeling, simulation and validation of a boiler drum: Some investigations”. In: *Energy* 126 (2017), pp. 312–325. DOI: <https://doi.org/10.1016/j.energy.2017.02.140>.
- [25] The International Association for the Properties of Water and Steam. *IAPWS Steam Tables*. URL: www.iapws.org.
- [26] Klaus Umminger et al. “Development of procedures for local void fraction measurements”. In: *Nuclear Engineering and Design* 336 (2018), pp. 163–170. DOI: <https://doi.org/10.1016/j.nucengdes.2018.05.014>. URL: <http://www.sciencedirect.com/science/article/pii/S0029549318305685>.
- [27] Adam Vaughan. *Germany agrees to end reliance on coal stations by 2038*. Visited: 30-01-19. 2019. URL: <https://www.theguardian.com/world/2019/jan/26/germany-agrees-to-end-reliance-on-coal-stations-by-2038>.
- [28] P. B. Whalley. *Boiling, condensation, and gas-liquid flow*. Oxford University Press, 2011. ISBN: 9780198562344.
- [29] Yu Zhao et al. “Void fraction measurement in steam–water two-phase flow using the gamma ray attenuation under high pressure and high temperature evaporating conditions”. In: *Flow Measurement and Instrumentation* 49 (2016), pp. 18–30. DOI: <https://doi.org/10.1016/j.flowmeasinst.2016.03.002>.
- [30] K.J. Åström and R.D. Bell. “Drum-boiler dynamics”. In: *Automatica* 36.3 (2000), pp. 363–378. DOI: [https://doi.org/10.1016/S0005-1098\(99\)00171-5](https://doi.org/10.1016/S0005-1098(99)00171-5).

Appendix A

Basic Theory

In this appendix the general theory of dynamic modelling is described. The derivation of the differential equations are also presented.

A.1 Dynamic Modelling Approach

To derive the state equations used for this thesis, the general way of describing the change over time in an arbitrary control volume is seen in Eq. A.1.

$$\text{Rate of accumulation} = \text{Rate entering the system} - \text{Rate leaving the system} + \text{Rate of generation within the system} \quad (\text{A.1})$$

This is the general equation that is used to derive the differential conservation equations used in this work.

A.1.1 Conservation of Mass

Conservation of mass is the basic for each of the elements used in the model developed. The conservation of mass determines how much mass is accumulated in the element which thereby determines the density of the fluid in the element. The conservation of mass is derived for a single dimensions, as only one dimension is used in this work. The flow of mass to a an arbitrary control volume is seen in Fig. A.1.

$$\frac{\partial \rho}{\partial t} + \frac{\partial(\rho u)}{\partial z} = 0 \quad (\text{A.2})$$

The partially derived continuity equation seen in Eq. A.2 is discretized for a control volume and denoted in terms of mass flow, yielding a simple expression that can be implemented.

$$\frac{dM}{dt} = \dot{m}_{in} - \dot{m}_{out} \quad (\text{A.3})$$

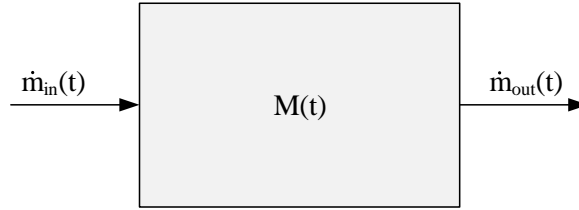


Figure A.1: Flow of mass for an arbitrary control volume.

A.1.2 Conservation of Energy

Conservation of energy is applied to all of the elements in the model. There are used two different state variables for the conservation of energy. For the water/steam side the state variable is enthalpy and for the flue gas and metal, the state variable is temperature. The conservation of energy is derived using the same methodology for both state equations.

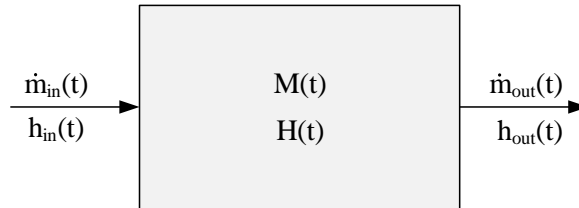


Figure A.2: Flow of energy for an arbitrary control volume.

The energy flow for an arbitrary control volume with one inlet and one outlet is seen in Fig. A.2. The differential equation is derived in a single dimension, since the assumptions stated in section 1.2.2 assumes that the flow is one-directional.

The first law of thermodynamics for an open system is applied to the arbitrary control volume yielding Eq. A.4.

$$\frac{dE}{dt} = \frac{d}{dt} \int_{V_{CV}} \rho \left(u + \frac{v^2}{2} + gz \right) dV_{CV} \quad (\text{A.4})$$

$$= \sum_k \left[\dot{m} \left(h + \frac{v^2}{2} + gz \right) \right]_k + \dot{Q} + \dot{W} - P \frac{dV_{CV}}{dt} \quad (\text{A.5})$$

The mechanical work, \dot{W} applied to the system is neglected. By neglecting the kinetic and potential energy contributions, the internal energy is used to simplify

Eq. A.5.

$$\frac{dU}{dt} = \sum_k [\dot{m}h]_k + \dot{Q} - P \frac{dV_{CV}}{dt} \quad (\text{A.6})$$

Assuming constant properties in the control volume Eq. A.6 is simplified further by knowing the internal energy is a function of the enthalpy, pressure and volume.

$$U = H - PV_{CV} \quad (\text{A.7})$$

$$\frac{dU}{dt} = \frac{dH}{dt} - P \frac{dV_{CV}}{dt} - V_{CV} \frac{dP}{dt} \quad (\text{A.8})$$

$$\frac{dH}{dt} = \sum_k [\dot{m}h]_k + \dot{Q} + V_{CV} \frac{dP}{dt} \quad (\text{A.9})$$

The thermal properties needed to calculate the enthalpy gradient are calculated using the approach as described in section 2.4.

A.2 Conservation of Momentum

Momentum conservation is very important for the natural circulation model. The density difference that drives the fluid around the circulation loop depends on the conservation of momentum. Since the pressure can change with the speed of sound, the conservation of equation is very difficult to calculate. The characteristic time for the momentum equation is much smaller than the characteristic time for the momentum and energy equations.

For an arbitrary control volume, seen in Fig. A.3, the forces acting on the volume is described as:

$$\frac{d}{dt} \int_{V(t)} \rho \mathbf{v} dV = \sum F \quad (\text{A.10})$$

When applying Leibnitz rule of integration for a volume and the divergence theorem, Eq. A.10 is divided into the following terms: [23].

$$\frac{d}{dt} \int_{V(t)} \mathbf{u} dV = \int_{V(t)} \frac{\partial \mathbf{u}}{\partial t} dV + \int_{S(t)} (\mathbf{n} \cdot \mathbf{v}_S) d\mathbf{u} dS \quad (\text{A.11})$$

$$\int_{V(t)} \nabla(\mathbf{v}\mathbf{u}) dV = \int_{S(t)} \mathbf{n} \cdot (\mathbf{v}\mathbf{u}) dS \quad (\text{A.12})$$

By combining Leibnitz rule and the divergence theorem, the equation yields:

$$\frac{d}{dt} \int_{V(t)} \mathbf{u} dV = \int_{V(t)} \left[\frac{\partial \mathbf{u}}{\partial t} + \nabla(\mathbf{v}\mathbf{u}) \right] dV \quad (\text{A.13})$$

By applying Reynolds transport theorem, the velocity vector is replaced by $\rho \mathbf{v}$, the bracket in Eq. A.13 is simplified:

$$\frac{\partial(\rho \mathbf{v})}{\partial t} + \nabla(\rho \mathbf{v}\mathbf{v}) = \mathbf{v} \left[\frac{\partial \rho}{\partial t} + \nabla \rho v \right] + \rho \left[\frac{\partial \mathbf{v}}{\partial t} + \mathbf{v} \cdot \nabla \mathbf{v} \right] \quad (\text{A.14})$$

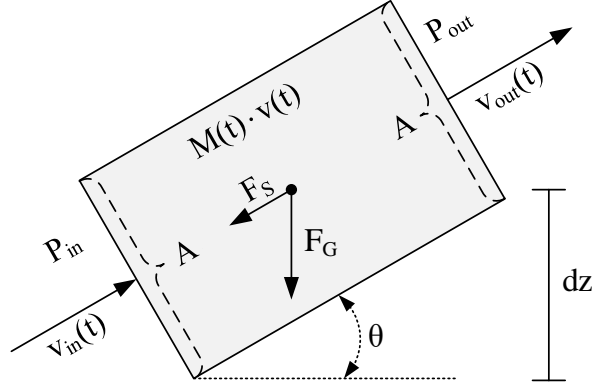


Figure A.3: Forces acting on an arbitrary control volume.

From the continuity equation in Eq. A.2, it is seen that the first term on the right-hand side in Eq. A.14 cancels out. When applying the material derivative, the conservation of momentum becomes.

$$\frac{d}{dt} \int_{V(t)} \rho \mathbf{v} dV = \int_{V(t)} \rho \frac{D\mathbf{v}}{Dt} dV \quad (\text{A.15})$$

The material/substantial derivative is defined as:

$$\frac{D}{Dt} \equiv \frac{\partial}{\partial t} + \nabla \mathbf{v} \quad (\text{A.16})$$

The momentum equation is now simplified to:

$$\int_{V(t)} \rho \frac{D\mathbf{v}}{Dt} dV = \sum F \quad (\text{A.17})$$

The sum of forces acting on the control volume is divided into two categories. The forces acting along the surface of the control volume and gravitational force acting on the entire volume. This is also seen in Fig. A.3.

$$\sum F = F_S + F_G \quad (\text{A.18})$$

The forces acting along the surface of the control volume is described by the pressure gradient over the control volume.

$$F_S = F_P + F_{P,loss} \quad (\text{A.19})$$

$$= A \frac{dP}{dz} - A \Delta P_{loss} \quad (\text{A.20})$$

$$= A (P_{in} - P_{out}) - A \Delta P_{loss} \quad (\text{A.21})$$

The pressure loss introduced in Eq. A.19 described for single-phase in section 2.4 and the two-phase pressure loss is described in appendix B. The gravitational force acting on the entire control volume for single-phase flow is described in Eq. A.22 and the two-phase gravitational term is described in appendix B.

$$F_G = A \cdot dz \cdot \rho \cdot g \cdot \sin \theta \quad (\text{A.22})$$

Inserting the forces into Eq. A.17, yields the expression that is then integrated over the entire volume. When the control volume is discretized into elements, the volume of each element is seen in Eq. A.23.

$$\int_{V=0}^{V=V} dV = V = A \cdot dz \quad (\text{A.23})$$

$$A \cdot dz \cdot \rho \frac{D\mathbf{v}}{Dt} = A (P_{in} - P_{out}) - A\Delta P_{loss} - A \cdot dz \cdot \rho \cdot g \cdot \sin \theta \quad (\text{A.24})$$

$$A \cdot dz \cdot \rho \left[\frac{\partial v}{\partial t} + v \frac{\partial v}{\partial z} \right] = A (P_{in} - P_{out}) - A\Delta P_{loss} - A \cdot dz \cdot \rho \cdot g \cdot \sin \theta \quad (\text{A.25})$$

By integrating over the entire length of the control volume, the partial derivatives are simplified.

$$v \frac{\partial v}{\partial z} = v \cdot \frac{v_{out} - v_{in}}{L} \quad (\text{A.26})$$

$$\frac{dv}{dt} + v \frac{v_{out} - v_{in}}{L} = \frac{P_{in} - P_{out} - \Delta P_{loss}}{\rho L} - g \sin \theta \quad (\text{A.27})$$

Appendix B

Theory of Two-Phase Flow

The fluid enters the downcomer as saturated liquid and is then subcooled due to the geodetic pressure of the water above. The subcooled water enters the evaporator and is then heated and at some point the fluid starts to boil. When boiling occurs there now exists two phases simultaneously in the pipes; the liquid phase and the gas phase. There are different ways of modelling the two phases co-existing in a pipe flow. One of the most used methods for such a flow is to treat the two phases as a homogeneous mixture and thereby assuming no slip between the phases. In this appendix one of the commonly used methods for calculating the pressure loss in a two-phase mixture is presented. Furthermore the heat transfer coefficient for two-phase water/steam mixture is presented. The method chosen is originally presented by Kandlikar and is chosen since it is easily implemented into an existing model.

The circulation of due to the density difference in the evaporator and downcomer, and not due to a pump circulation, the flow is still considered a forced flow. It is very difficult to control the flow of water in the riser tubes, but since the flow is moving inside a pipe, the flow is considered forced. Initially when the water starts to boil, there are formed small bubbles which groups into larger formations called slugs. Both the bubbles and slugs move faster than the fluid due to the lower density of the steam. This is called slip and in this work it is assumed that the liquid and gas phase move at the same velocity.

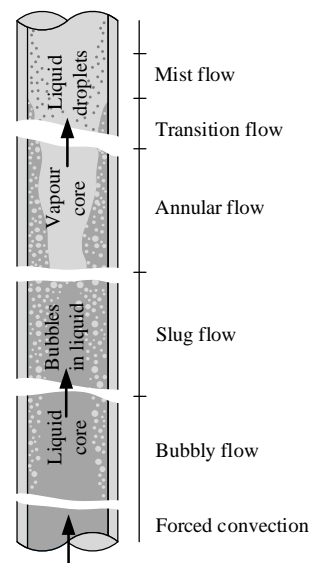


Figure B.1: Boiling regimes in a two-phase flow.

B.1 Pressure loss in a homogeneous two-phase mixture

There are a number of classical methods of calculating the pressure loss in a two-phase water/steam mixture. One of the most widely used methods is to use flow frictional multipliers originally presented by Collier and Thome [7]. The flow frictional multiplier is simply multiplied with the single-phase liquid frictional pressure loss and thereby obtaining the two-phase pressure loss. This method is widely used since it is easily implemented into existing models.

Another widely used methods is to use the separated flow model and assuming a homogeneous mixture. By using the pressure loss gradients also described by Whalley [28] an explicit expression can be obtained for the two-phase mixture.

The pressure loss gradient in a 1-dimensional flow is presented by Whalley as Eq. B.1.

$$-\frac{dP}{dz} = \underbrace{f \cdot \frac{1}{D} \cdot \frac{\dot{G}^2}{2 \cdot \rho_h}}_{\text{Frictional term}} + \underbrace{\rho_h \cdot g \cdot \sin \theta}_{\text{Gravitational term}} + \underbrace{\dot{G}^2 \cdot \frac{d}{dz} \left(\frac{1}{\rho_h} \right)}_{\text{Acceleration term}} \quad (\text{B.1})$$

If Eq. B.1 is integrated over the entire pipe length, an explicit expression for the pressure loss gradient is obtained.

$$-\Delta P = - \int_{z=0}^{z=L} \left(\frac{dP}{dz} \right) dz = \int_{z=0}^{z=L} \left(\frac{dP}{dz} \right)_F dz + \int_{z=0}^{z=L} \left(\frac{dP}{dz} \right)_G dz + \int_{z=0}^{z=L} \left(\frac{dP}{dz} \right)_A dz \quad (\text{B.2})$$

The total pressure loss is divided into three subterms; the frictional pressure loss, the gravitational pressure difference and the pressure difference due to acceleration of the fluid.

The frictional term is can be obtained by integrating over the length.

$$\Delta P_F = \int_{z=0}^{z=L} \left(\frac{dP}{dz} \right)_F dz = f \frac{\dot{G}^2}{2 \cdot D} \int_{z=0}^{z=L} \left(\frac{1}{\rho_H} \right) dz \quad (\text{B.3})$$

Assuming a constant friction factor for the pipe length, the frictional pressure loss becomes a function of the homogeneous density over the pipe length. The homogeneous density is defined as Eq. B.4.

$$\frac{1}{\rho_H} = \frac{x}{\rho_v} + \frac{1-x}{\rho_L} \quad (\text{B.4})$$

By inserting Eq. B.4 into Eq. B.3, the expression is now a function of the steam mass fraction.

$$\Delta P_F = f \frac{\dot{G}^2}{2 \cdot D} \int_{z=0}^{z=L} \left(\frac{x}{\rho_v} + \frac{1-x}{\rho_L} \right) dz \quad (\text{B.5})$$

Assuming the steam mass fraction is a linear function of the pipe length, Eq. B.6 is obtained.

$$x = \frac{x_{out}}{L} \cdot z \quad (\text{B.6})$$

Eq. B.5 can now be integrated for the pipe length, as seen in Eq. B.7.

$$\Delta P_F = f \frac{\dot{G}^2 \cdot L}{2 \cdot D} \cdot \left(\frac{1}{\rho_L} \right) \left(\frac{x_{out}}{2} \left(\frac{\rho_L - \rho_V}{\rho_V} \right) + 1 \right) \quad (\text{B.7})$$

To simplify Eq. B.7, the dimensionless density weight function X_0 is defined.

$$X_0 = x_{out} \left(\frac{\rho_L - \rho_V}{\rho_V} \right) \quad (\text{B.8})$$

By using the dimensionless density weight function, Eq. B.7 is simplified to:

$$\Delta P_F = f \frac{\dot{G}^2 \cdot L}{2 \cdot D} \cdot \left(\frac{1}{\rho_L} \right) \left(1 + \frac{X_0}{2} \right) \quad (\text{B.9})$$

Using the same methodology an explicit expression is derived for the gravitational and acceleration term. In Eq. B.10 the gravitational term is integrated over the length of the pipe.

$$\Delta P_G = \int_{z=0}^{z=L} \left(\frac{dP}{dz} \right)_G = \int_{z=0}^{z=L} (g \cdot \sin \theta \cdot \rho_H) dz = g \cdot \sin \theta \int_{z=0}^{z=L} (\rho_H) dz \quad (\text{B.10})$$

Eq. B.4 is the inverse of the homogeneous density, and it is therefore rewritten to suit Eq. B.10.

$$\frac{1}{\rho_H} = \frac{x \cdot (\rho_L - \rho_V) + \rho_V}{\rho_V \cdot \rho_L} \quad (\text{B.11})$$

$$\rho_H = \frac{\rho_V \cdot \rho_L}{x \cdot (\rho_L - \rho_V) + \rho_V} \quad (\text{B.12})$$

The expression for the homogeneous density is inserted into Eq. B.10 and the intergration is performed.

$$\Delta P_G = g \cdot \sin \theta \int_{z=0}^{z=L} \left(\frac{\rho_V \cdot \rho_L}{x \cdot (\rho_L - \rho_V) + \rho_V} \right) dz \quad (\text{B.13})$$

$$= g \cdot \sin \theta \cdot \rho_V \cdot \rho_L \int_{z=0}^{z=L} \left(\frac{1}{x \cdot (\rho_L - \rho_V) + \rho_V} \right) dz \quad (\text{B.14})$$

$$= g \cdot \sin \theta \cdot \rho_V \cdot \rho_L \int_{z=0}^{z=L} \left(\frac{1}{x_{out}/L \cdot (\rho_L - \rho_V) + \rho_V} \right) dz \quad (\text{B.15})$$

Finally given the explicit expression for the gravitational pressure difference for a homogeneous two-phase mixture.

$$\Delta P_G = g \cdot \sin \theta \cdot \rho_L \cdot L \left(\frac{\ln(1 + X_0)}{X_0} \right) \quad (\text{B.16})$$

The same methodology is applied for the acceleration term, starting with the ODE and integrating over the length of the pipe.

$$\Delta P_A = \int_{z=0}^{z=L} \left(\frac{dP}{dz} \right)_A dz \quad (\text{B.17})$$

$$= \int_{z=0}^{z=L} \left(\dot{G}^2 \frac{d}{dz} \left(\frac{1}{\rho_H} \right) \right) dz \quad (\text{B.18})$$

$$= \dot{G}^2 \int_{z=0}^{z=L} \left(\frac{d}{dz} \left(\frac{1}{\rho_H} \right) \right) dz \quad (\text{B.19})$$

The homogeneous density function in Eq. B.4 is used once again and the linear expression for the steam mass fraction as function of the pipe length is also introduced.

$$\frac{1}{\rho_H} = \frac{x}{\rho_V} + \frac{1-x}{\rho_L} \quad (\text{B.20})$$

$$= \frac{x_{out}}{L \cdot \rho_V} \cdot z + \frac{1}{\rho_L} - \frac{x_{out}}{L \cdot \rho_L} \cdot z \quad (\text{B.21})$$

Eq. B.21 is then differentiated in order to be used in Eq. B.19.

$$\frac{d}{dz} \left(\frac{1}{\rho_H} \right) = \frac{x_{out}}{L \cdot \rho_V} - \frac{x_{out}}{L \cdot \rho_L} \quad (\text{B.22})$$

Using the differentiated steam mass fraction, the pressure difference due to acceleration is intergrated over the pipe length.

$$\Delta P_A = \dot{G}^2 \left[\frac{x_{out}}{L \cdot \rho_V} \int_{z=0}^{z=L} dz - \frac{x_{out}}{L \cdot \rho_L} \int_{z=0}^{z=L} dz \right] \quad (\text{B.23})$$

$$= \dot{G}^2 \left[\frac{x_{out}}{L \cdot \rho_V} \cdot L - \frac{x_{out}}{L \cdot \rho_L} \cdot L \right]_{z=0}^{z=L} \quad (\text{B.24})$$

$$= \dot{G}^2 \left[x_{out} \left(\frac{1}{\rho_V} - \frac{1}{\rho_L} \right) \right] \quad (\text{B.25})$$

Once again the density weight function X_0 is used to simplify the explicit function. The final simplified expression is then seen in Eq. B.26

$$\Delta P_A = \dot{G}^2 \frac{X_0}{\rho_L} \quad (\text{B.26})$$

The total pressure difference over a pipe length is the sum of the derived explicit expressions and is seen in Eq. B.27

$$-\Delta P = f \frac{\dot{G}^2 \cdot L}{2 \cdot D} \cdot \left(\frac{1}{\rho_L} \right) \left(1 + \frac{X_0}{2} \right) + g \cdot \sin \theta \cdot \rho_L \cdot L \left(\frac{\ln(1 + X_0)}{X_0} \right) + \dot{G}^2 \frac{X_0}{\rho_L} \quad (\text{B.27})$$

B.2 Heat transfer in two-phase flows

The heat transfer in the internal pipe flow is described by Newton's law of cooling also seen in Eq. 2.45. The heat transfer depends on the temperature of the two mediums and the heat transfer coefficient. For a single-phase flow the Nusselt number can be calculated using the Dittus-Boelter equation as described in section 2.4. The heat transfer coefficient for a two-phase mixture of water and steam is a more difficult to calculate since boiling occurs simultaneously. Investigating the literature there are different approximations for calculating the heat transfer for such a case, and some studies assumes a large heat transfer coefficient ($h_{2P} > 10000$ W/m²K) [23]. For this study a general correlation for vertical pipes proposed by Kandlikar [15] is used. The correlation is based on 5246 data points and an mean deviation of 15.9 % is achieved. The correlation is based on the liquid heat transfer coefficient being multiplied with a convective number and boiling number.

The proposed methods for calculating the heat transfer coefficient for a two-phase water/steam mixture is seen in Eq. B.28.

$$h_{2P} = \underbrace{C_1 Co^{C_2} h_L}_{\text{Convective boiling}} + \underbrace{C_3 Bo^{C_4} h_L}_{\text{Nucleate boiling}} \quad (\text{B.28})$$

Where the coefficient used are defined as a function of the convective number, which can be seen in Tab. B.1. The convective number is defined using Eq. B.29

Table B.1: Constants used in the general correlation proposed by Kandlikar [15].

| Constant | Convective region | Nucleate boiling region |
|----------|-------------------|-------------------------|
| C_1 | 1.1360 | 0.6683 |
| C_2 | -0.9 | -0.2 |
| C_3 | 667.2 | 1058.0 |
| C_4 | 0.7 | 0.7 |

and then boiling number is defined using Eq. B.30.

$$Co = \left(\frac{1-x}{x} \right)^{0.8} + \left(\frac{\rho_V}{\rho_L} \right)^{0.5} \quad (\text{B.29})$$

$$Bo = \frac{\dot{q}}{\dot{G}h_{lg}} \quad (\text{B.30})$$

The heat flux needs to be iterated, since the heat flux applied is a function of the heat transfer coefficient. Therefore the a small iterative loop is made, and it converges within a few iterations.

The issue when using this approach is that when the fluid crosses the saturation line, this methods is not suitable before a steam mass fraction of approximately 0.1 % is achieved. Therefore the statement seen in Eq. B.31 is used when calculating the heat transfer coefficient.

$$h_{2P} = \begin{cases} 4500 & \text{for } 0 < x < 0.001 \\ \text{Eq. B.28} & \text{for } 0.001 < x < 1 \end{cases} \quad (\text{B.31})$$

Appendix C

Flue Gas Properties

To calculate the flue gas properties different methods are proposed in literature. One of the most used is the NASA polynomials for individual species [12]. The NASA polynomials is a collection of coefficients for individual gas species where a number of thermal properties and transport properties can be calculated from. The NASA polynomials are easily implemented into a model due to the simplicity of the polynomials.

The thermal conductivity, specific heat capacity and viscosity are calculated using the NASA polynomials, and the proposed polynomials are seen in Eq. C.1, C.2 and C.3 respectively.

$$\ln(k_{gas}) = a \cdot \ln T + \frac{b}{T} + \frac{c}{T^2} + d \quad (C.1)$$

$$c_{p,gas} = a + b \cdot T + c \cdot T^2 + d \cdot T^3 + e \cdot T^4 \quad (C.2)$$

$$\ln(\mu_{gas}) = a \cdot \ln T + \frac{b}{T} + \frac{c}{T^2} + d \quad (C.3)$$

The flue gas is a mixture of individual species where the dominating ones are nitrogen, carbon dioxide, water vapour and, depending on the excess air ratio, oxygen. The coefficients for each of the species are not presented in this appendix due to the length of each coefficient.

The properties for the gas mixture is then calculated using the mass weight average function as seen in Eq. C.4-C.7, where χ denotes the mass fraction of each individual species.

$$c_p = \sum_{i=1}^n c_{p,i} \cdot \chi_i \quad (\text{C.4})$$

$$\mu = \sum_{i=1}^n \mu_i \cdot \chi_i \quad (\text{C.5})$$

$$k = \sum_{i=1}^n k_i \cdot \chi_i \quad (\text{C.6})$$

$$\rho = \sum_{i=1}^n \rho_i \cdot \chi_i \quad (\text{C.7})$$

Appendix D

Mathematical Model of Natural Circulation Biomass Boilers during Start-Up

K. Bilde, K. Sørensen, T. Condra

The paper has been submitted to the International Journal of Heat and Mass Transfer for peer-review

Mathematical Model of Natural Circulation Biomass Boilers during Start-Up

Kasper Gram Bilde^{1,*}, Kim Sørensen¹, Thomas Condra¹

Aalborg University, Department of Energy Technology, Pontoppidanstræde 111, 9220 Aalborg, Denmark

Abstract

A natural circulation biomass boiler is a highly dynamic system, especially during start-up where the entire system is initially cold. During a start-up procedure, swelling of water inside the steam drum is often experienced due to the evaporation and expansion of the water. A mathematical model describing the dynamics of a natural circulation evaporator is presented. The complex geometry of the biomass boiler is simplified to 300 parallel tubes, which are discretized in one dimension. The model captures the evaporation of water and the dynamic instabilities introduced by density wave oscillations. During the phase transition into the two-phase regime, the steam produced displaces water, causing the water level in the steam drum to rise rapidly. The rapid increase in water level is observed every time boiling occurs in the discretized elements. The fast dynamic instabilities encountered during a start-up procedure are important to resolve since the dynamic instabilities have a large impact on the water level inside the steam drum.

Keywords: Two-phase flow, Steam drum, Natural circulation, Dynamic simulation, Dynamic instability, Cold start-up, Evaporator, Swelling

1. Introduction

Reliable start-up procedures are important for any steam power plant operator. During a cold start-up, the boiler plant is highly dynamic and the water level inside the steam drum is difficult to control. The circulation of water in a natural circulation biomass boiler is not driven by a pump but through the density difference between the cold water entering the downcomer and the water/steam mixture leaving the evaporator tubes. Therefore the evaporation of water in the evaporator is one of the key factors when simulating the water level inside the steam drum since steam displaces water under boiling and this causes a sudden increase in the water level in the steam drum. A biomass boiler differs from other types of boilers since the time it takes to fully burn the fuel takes a number of minutes compared to for example a gas- or oil-fired boiler, where the fuel is burned in a matter of seconds. The firing in a biomass boiler thus has a longer response time compared to other types of boilers, which makes it more difficult to control. The model presented in this work is made for a biomass boiler burning waste-wood with a thermal firing capacity of 125 MW and is designed to deliver steam to a steam turbine with a pressure of 92 bar_a and a temperature of 477°C.

The dynamic performance of steam boilers has been the subject of many studies over the last +30 years. The dynamic models developed have been continuously improved to adapt to different situations and different types of boilers. Elmegaard [1] developed a general tool to simulate the dynamic performance of boilers. The author developed a flexible model, named DNA,

that is capable of simulating the dynamic performance of an energy system. The DNA tool consists of a component library where most energy system can be simulated under the developed conditions. The methodology used to develop the components of the boiler can be used to dynamically model many different energy systems. The mathematical modelling methodology is used in this work.

One of the most widely used studies when modelling boilers with a steam drum is the model developed by Åström and Bell [2]. The model developed is able to simulate the water level inside the steam drum when a plant has experienced a change in operational load. The model consists of explicit expressions making it easy to implement into other models, and this is also why this model is one of the most widely used. The limitations of the work are that no subcooling of water is taken into consideration. It is assumed that the water entering the riser tubes is saturated water.

Using a similar approach, Adam and Marchetti [3] developed a model describing the dynamics of a steam drum with the focus on designing a water level controller. The controller is able to control the water level inside the steam drum. At each time step, the momentum equation is solved in steady state assuming that the pressure changes happen instantaneously. The assumption that the pressure changes instantaneously limits the work to be used in a dynamic model describing the start-up procedure where the pressure is increased over time, e.g. a start-up procedure.

Kim and Choi [4] expanded the model proposed by Åström and Bell [2] to describe the condensation occurring below the water level inside the steam drum. The work has a main focus on the steam drum and it is therefore assumed that the momentum equation of the recirculation loop is solved in steady

*Corresponding author

Email addresses: kasperbilde@gmail.com (Kasper Gram Bilde), kso@et.aau.dk (Kim Sørensen), tc@et.aau.dk (Thomas Condra)

Nomenclature

Dimensionless Numbers

| | |
|------|-----------------|
| Nu | Nusselt number |
| Pr | Prandtl number |
| Re | Reynolds number |

Greek Symbols

| | |
|--------|---------|
| ρ | Density |
|--------|---------|

Latin Symbols

| | |
|-------|----------------------------|
| A | Area |
| f | Darcy friction factor |
| g | Gravitational acceleration |
| H | Enthalpy |
| h | Specific enthalpy |
| K_L | Minor loss coefficient |
| L | Length |
| M | Mass |
| m | Mass flow |
| P | Pressure |
| Q | Heat flow |
| T | Temperature |
| t | Time |

| | |
|-----|---------------------|
| V | Volume |
| v | Velocity |
| x | Steam mass fraction |

Subscripts

| | |
|-------|--------------|
| A | Acceleration |
| D | Drum |
| dc | Downcomer |
| F | Friction |
| f | Fluid |
| fg | Flue gas |
| fw | Feedwater |
| G | Gravitation |
| i | Index |
| in | Inlet |
| L | Liquid |
| r | Risers |
| s | Surface |
| sat | Saturation |
| V | Vapour |
| w | Wall |

state. The model developed by Kim and Choi [4] describes the dynamics of a steam drum accurately. The limitations of the work are that no subcooling of water is taken into consideration, thereby assuming the water enters the riser tubes as saturated liquid.

A fast dynamic model is developed by Sedic et al. [5] to describe the overall performance of a natural circulation boiler with a steam drum. The proposed model discretizes the evaporator into 5 elements and solves the dynamic mass, energy and momentum conservation equations for all elements. The model is developed with a focus on controlling the water level inside the steam drum and a PI controller is therefore implemented. The model is tested for plants operating at a certain load and analysing the changes occurring when a change in load is experienced.

Johansen et al. [6] have made extensive work simulating the dynamic performance of once-through Benson boilers. In a Benson boiler, the feedwater enters the evaporator as subcooled water and is then evaporated through the evaporator. When the fluid reaches saturation the flow could oscillate due to the phase transition [7], and a solver capable of handling these oscillations is developed. To achieve a high computational speed, Johansen et al. [6] propose to use a look-up interpolation table to calculate the properties of water.

Alobaid et al. [8] presented a model describing the dynamics of a 60 MW_{th} municipal solid waste (MSW) incinerator. The

simulation of the flue gas side is of great interest to the authors and a lot of effort is made to describe the flue gas and combustion of the solid waste accurately. The model is developed using the simulation software APROS. The model presented is able to simulate the MSW incinerator with an error percentage of 5 %.

When simulating the transient phase transition of a fluid, dynamic instabilities are often experienced. Kakac and Bon [9] made an extensive review describing the physical phenomena of steady-state instabilities and dynamic instabilities. Simulating a dynamic system, such as a natural circulation boiler, dynamic instabilities are often experienced. During the transition between the single-phase regime and the two-phase regime, the density of water decrease to roughly 1/100 of the initial density, resulting in a much higher velocity. This increased velocity causes density wave oscillations (DWO) and pressure oscillations due to an increased pressure gradient. The dynamic instabilities for such a dynamic system are important to resolve since the small time step where boiling occurs has a large impact on the water level in the steam drum.

The void fraction of steam in a tube is one of the most important parameters when characterising a two-phase flow. The void fraction can be determined experimentally using an x-ray- or gamma-ray attenuation system ([10], [11]). The experimental method has been developed since the 1960s and in modern times it is a tool for determining the void fraction of a two-phase

mixture quite accurately. Zhao et al. [12] used the gamma-ray attenuation system to determine the void fraction of steam in a water/steam mixture under high pressure and high temperature during evaporating conditions. The authors compared the obtained experimental results to some of the most commonly used void fraction correlation. Using a similar approach, Nazami et al. [13] determined the void fraction of an oil/gas mixture. The authors determine the flow boiling regime as well as the void fraction. Furthermore, a neural network is developed to obtain fast and reliable void fraction using a minimum of inputs.

In this study, a model to simulate the performance of a natural circulation evaporator during a cold start-up is presented. Until saturation is reached, the water circulates in the evaporation loop applying sufficient cooling of the water walls. When steam is produced, the pressure inside the system can be increased following a maximum allowable temperature gradient due to the possibility of thermal stress in the thick-walled components such as the steam drum. The maximum allowable temperature gradient is usually a conservatively low gradient in practice, but Taler et al. [14] investigated the thermal stress experienced in the thick-walled components and optimised the maximum allowable temperature gradient, which reduced the start-up time. A maximum allowable temperature gradient is used to ensure a sufficiently low thermal stress. When the fluid transitions into the two-phase regime, the steam produced displaces the liquid, causing an increased mass flow out of the discretized element. The increased mass flow causes sudden swelling in the steam drum. The model developed includes the downcomers, evaporators and steam drum. The entire model is developed as one-dimensional.

2. Modelling Approach

The geometry of a natural circulation biomass boiler is complex, due to the many bends and tubes connected in the system. A typical three-pass boiler is seen in Fig. 1 and it can be seen that the furnace, first- and second pass is enclosed in water walls. The water walls act as the evaporator of the system, ensuring a sufficiently low wall temperature. In this work, the water walls are neglected in the first- and second pass, due to the low flue gas temperature in these passes during the cold start-up of the boiler. The main heat transfer is occurring in the furnace of the boiler, and the geometry of the boiler is thereby simplified. For this work, the impact of the superheaters and economisers are neglected, and it is assumed that the water entering the steam drum is saturated liquid.

The complex geometry of a natural circulation steam boiler is simplified to the geometry seen in Fig. 2. The system is divided into three groups; steam drum, downcomer and evaporator. The differential and algebraic equations describing the groups are presented in the following section. The simplified natural circulation loop, seen in Fig. 2, is discretized into a number of elements, and 300 parallel tubes are modelled. Each parallel tube is subject to the same amount of heat.

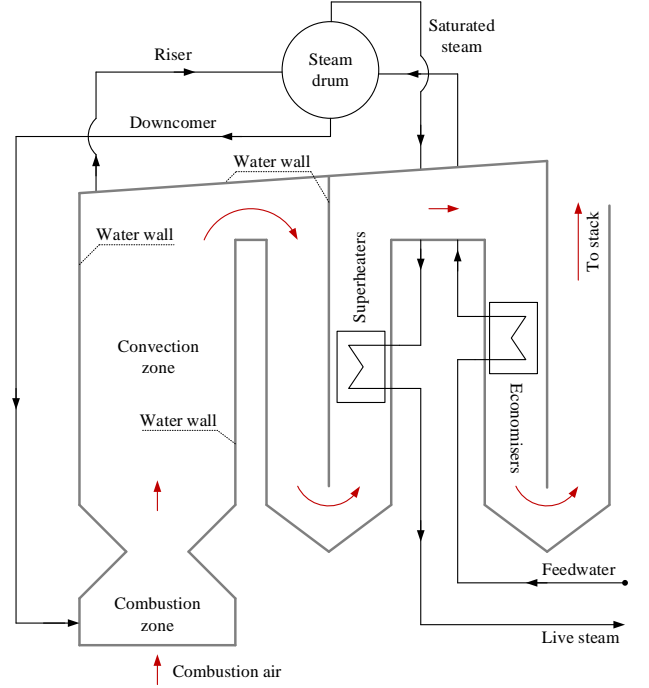


Figure 1: Complex geometry of a natural circulation biomass boiler with three passes.

2.1. Differential Equations for Downcomer

The downcomer is discretized into n 1-dimensional elements in order to convert the energy, mass and momentum PDEs to ODEs. To each element the three conservation equations are applied as seen in Eqs. 1, 2 and 3 respectively.

$$\frac{dM_i}{dt} = \dot{m}_{i-1} - \dot{m}_i \quad (1)$$

$$\frac{dH_i}{dt} = \dot{m}_{i-1}h_{i-1} - \dot{m}_i h_i + V_i \frac{dP_i}{dt} \quad (2)$$

$$\frac{d\bar{v}_i}{dt} = \frac{P_i - P_{i+1} - \Delta P_i}{\bar{\rho}_i \cdot L_i} + \bar{v}_i \frac{v_{i-1} - v_i}{L_i} + g \quad (3)$$

2.2. Differential Equations for Evaporator

The evaporator is also discretized into n 1-dimensional elements yielding a total of $2n$ elements. The difference between the downcomer and evaporator is that heat is applied to the evaporator elements and gravity works in opposing directions. The three conservation equations are applied to each evaporator element, as seen in Eqs. 4, 5 and 6.

$$\frac{dM_i}{dt} = \dot{m}_{i-1} - \dot{m}_i \quad (4)$$

$$\frac{dH_i}{dt} = \dot{m}_{i-1}h_{i-1} - \dot{m}_i h_i + \dot{Q}_i + V_i \frac{dP_i}{dt} \quad (5)$$

$$\frac{d\bar{v}_i}{dt} = \frac{P_i - P_{i+1} - \Delta P_i}{\rho_i \cdot L_i} + \bar{v}_i \frac{v_{i-1} - v_i}{L_i} - g \quad (6)$$

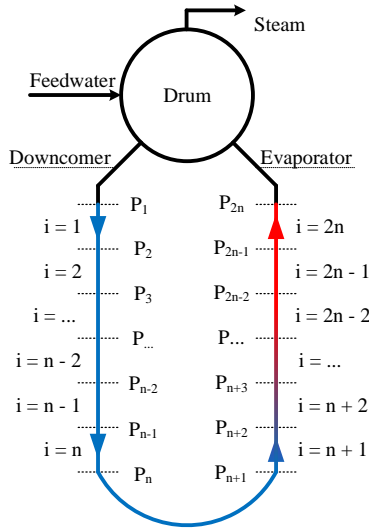


Figure 2: Simplified boiler with discretization of downcomer and evaporator.

The differential equations presented for both the downcomer and the evaporator are solved using MATLAB's built-in ODE solver *ODE15s*. The *ODE15s* solver is used due to the stiff system of equations introduced by the momentum equation ([15], [16]). The time constant related to the momentum equation is much smaller compared to the continuity and energy equation (order of the speed of sound).

2.3. Algebraic Equations for Recirculation Loop

At each time step, the following algebraic equations are solved to calculate the gradients used in the ODEs.

To calculate the pressure in each element at least two thermodynamic properties of water has to be calculated. The density and specific enthalpy are calculated from the state variables for each element, as seen in Eqs. 7 and 8.

$$\bar{\rho}_i = \frac{M_i}{V_i} \quad (7)$$

$$\bar{h}_i = \frac{H_i}{M_i} \quad (8)$$

The mean pressure in each element is then calculated using the IAPWS-IF97 steam tables [17], and the pressure is calculated iteratively as a function of the mean specific enthalpy and mean density, as seen in Eq. 9. The IAPWS-IF97 steam table is used in a MATLAB format developed by Holmgren [18] and is called X Steam. The pressure is iteratively calculated with low convergence criteria to ensure consistency when the fluid is in the vicinity of the saturation line. Other authors, such as Johansen et al. [6] and the International Association for the Properties of Water and Steam, [19], proposes the use of an interpolation look-up method for calculating the pressure as a function of the density and specific enthalpy/internal energy for a faster computational time. For this work, the iterative pressure solver developed was sufficiently fast.

$$\bar{P}_i = f(\bar{\rho}_i, \bar{h}_i) \quad (9)$$

The in- and outlet pressures of each discretized element are linearly interpolated using the mean pressure.

$$P_{out,i} = 2\bar{P}_i - P_{in,i} \quad (10)$$

The pressure gradient in each element is evaluated using a homogeneous mixture model [20]. The classic separated pressure gradient models, also described by Whalley [21], is not applied and therefore there is no slip between the two phases. Furthermore, a void fraction is not calculated due to the homogeneous assumption. The homogeneous mixture model is only applied when there is steam present in the flow, otherwise, the single-phase pressure gradient correlation is applied [22]. If the separated model were to be used, the slip between the two phases and the void fraction of steam have to be taken into account, which has the largest impact at low pressures. Since the boiler reaches a relatively high pressure rapidly, the homogeneous assumption with no slip is acceptable, since the slip between the two phases become less dominating. This is especially the case when the steam mass fraction is low, which is the case during a start-up procedure.

$$\Delta P_i = \begin{cases} \left(f \cdot \frac{L_i}{D} + \sum_k K_L \right) \frac{1}{2} \cdot \bar{\rho}_i \cdot \bar{v}_i & \text{for single-phase} \\ \Delta P_F + \Delta P_A + \Delta P_G & \text{for two-phase} \end{cases} \quad (11)$$

The heat transferred to the fluid is calculated using the Dittus-Boelter equation for the single-phase flow [22], also seen in Eq. 12.

$$Nu = 0.023 \cdot Re^{0.8} \cdot Pr^{0.4} \quad (12)$$

For the two-phase mixture, the heat transfer coefficient is calculated using a general correlation for vertical tubes proposed by Kandlikar [23]. The two-phase heat transfer coefficient is a function of the heat flux and therefore needs to be iterated to convergence. The correlation is chosen instead of using a high heat transfer coefficient ($h_{inner} > 10^4 \text{ W/m}^2\text{K}$) since it is easily implemented. The internal heat transfer is much larger than the outer heat transfer coefficient, which is of the order of $h_{outer} \approx 10^2 \text{ W/m}^2\text{K}$.

2.4. Differential Equations for the Steam Drum

The overall continuity and energy differential equations for the steam drum are seen in Eqs. 13 and 14 respectively. The in- and outlets from the steam drum can also be seen inspecting Fig. 3.

$$\frac{dM_D}{dt} = \dot{m}_{fw} + \dot{m}_r - \dot{m}_{dc} - \dot{m}_s \quad (13)$$

$$\frac{dH_D}{dt} = \dot{m}_{fw}h_{fw} + \dot{m}_r h_r - \dot{m}_{dc}h_{dc} - \dot{m}_s h_s \quad (14)$$

Since the steam drum separates the vapour produced in the riser from the liquid, two phases exist in the steam drum simultaneously. The two phases are treated separately and it is assumed that no condensation of steam takes place in the steam drum. The continuity and energy equations for the liquid phase are seen in Eqs. 15 and 16. The continuity and energy equations

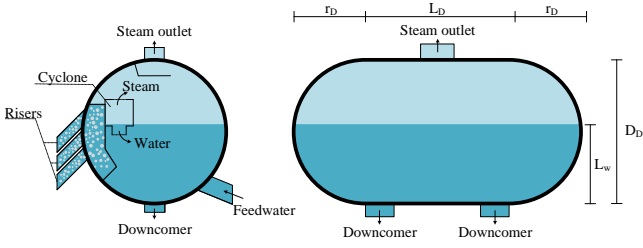


Figure 3: Simplified geometry of the steam drum. The water and steam are separated using the cyclone in the steam drum.

for the vapour phase are seen in Eqs. 17 and 18 respectively. For both phases the mass fraction of steam is used to determine the amount of steam leaving the riser tubes.

$$\frac{dM_{LD}}{dt} = \dot{m}_{f_w} + (1 - x_r) \cdot \dot{m}_r - \dot{m}_{dc} \quad (15)$$

$$\frac{dH_{LD}}{dt} = \dot{m}_{f_w} h_{f_w} + (1 - x_r) \cdot \dot{m}_r h_r - \dot{m}_{dc} h_{dc} + V_{LD} \frac{dP_D}{dt} \quad (16)$$

$$\frac{dM_{VD}}{dt} = x_r \cdot \dot{m}_r - \dot{m}_s \quad (17)$$

$$\frac{dH_{VD}}{dt} = x_r \cdot \dot{m}_r h_r - \dot{m}_s h_s + V_{VD} \frac{dP_D}{dt} \quad (18)$$

2.5. Algebraic equations for the Steam Drum

The pressure in the steam drum is regulated using an ideal steam valve. The ideal steam valve is able to control the temperature gradient of the steam drum without the practical constraints of a real valve. Steam can, therefore, leave the steam drum at any desired rate and does not have to follow the valve characteristics of for example a linearly controlled valve. The pressure is controlled using a maximum allowable temperature gradient of 2.5 K/min [24]. The maximum allowable pressure increase is calculated using Eq. 19.

$$\left. \frac{dP_D}{dt} \right|_{\max} = \frac{P_{sat}(T + dT) - P_{sat}(T)}{dT} \quad (19)$$

The water level inside the steam drum is calculated using the mass, pressure and geometry of the steam drum seen in Fig. 3. The volume of the fluid is a function of the actual pressure inside the steam drum, as seen in Eq. 20.

$$V_f(P_D, t) = \underbrace{\frac{M_{LD}(t)}{\rho_L(P_D)}}_{V_L} + \underbrace{\frac{M_{VD}(t)}{\rho_V(P_D)}}_{V_V} \quad (20)$$

The liquid volume occupying the steam drum gives the water level using the geometry of a partially filled volume.

The steam drum water level is regulated using an ideal feedwater valve. This is introduced in order to have a steady desired water level inside the steam drum. By having a steady water level inside the steam drum, the impact of the rapid changes in

water level can easily be observed. The steam leaving the steam drum is regulated using the maximum allowable pressure gradient and the volume of the steam drum. At each time, the volume of steam that cannot be stored inside the steam drum leaves the steam drum, assuming an ideal steam valve. The ideal steam valve allows the maximum allowable pressure gradient to be followed.

2.6. 1-D Wall Model

The tube walls act as a thermal resistance between the flue gas and the water/steam mixture inside the riser tubes. The tube wall is modelled in 1-D just as the fluid flowing inside the tubes. The tube wall is subject to the differential energy equation, seen in Eq. 21. No momentum or mass is transferred to the tube wall. The chosen independent variable is the temperature of the tube wall.

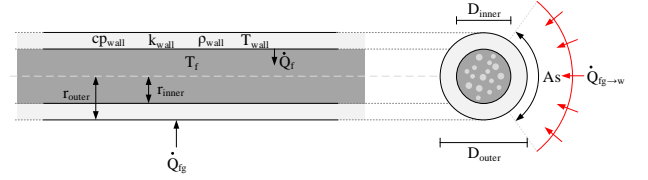


Figure 4: Tube wall model. Heat is applied to the surface of the tube that is exposed to the flue gas.

$$M_w \cdot c_{p,w} \cdot \frac{dT_w}{dt} = \dot{Q}_{fg \rightarrow w} - \dot{Q}_f \quad (21)$$

$$= h_{fg} \cdot A_s \cdot (T_{fg} - T_w) - h_f \cdot A_s \cdot (T_w - T_f) \quad (22)$$

The walls are assumed to be very thin, thereby neglecting the thermal conduction taking place inside the walls. The thermal inertia of the metal is taken into consideration, as seen in Eq. 21.

3. Results and Discussion

Heat is applied after 10 seconds of simulation time and the heat applied is increased linearly over time. The 10 seconds of simulation time without heat applied, ensures that the system is initially at rest. When heat is applied, the density of the water decreases, and the circulation of water starts. The water is heated until saturation is reached. During this time the circulation of water heats the steam drum and the temperature gradient of the steam drum is only a function of the heat input and pressure loss coefficients. For large pressure loss coefficients, the velocity of the fluid is lower, and the fluid has a longer residence time in the evaporator. When saturation is reached, the water will transition into the two-phase regime, at the discretized tube length, and boiling occurs. Fig. 5 shows how the fluid starts to boil in the water walls. Boiling is first observed in the top element, then at the second top element and

so forth. When boiling occurs, steam is produced and the pressure inside the system can be increased. This is also why there is a different time span between the boiling sequences. When the boiler has transitioned to steady-state operation, the mass fraction of steam leaving the evaporator is $x_{evap,out} \approx 5\%$.

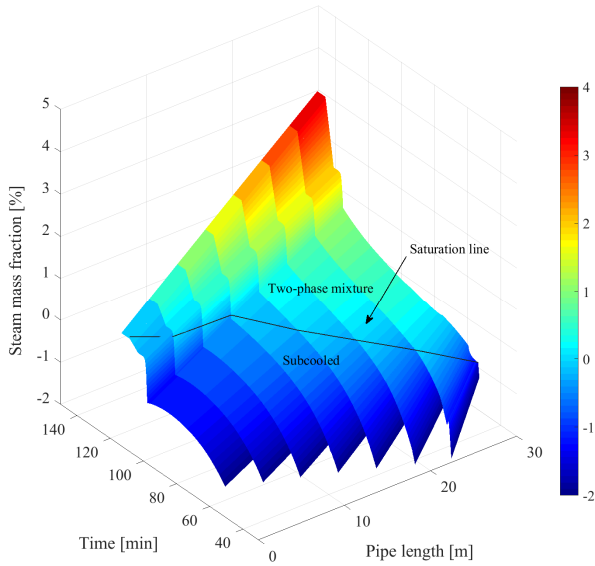


Figure 5: Mass fraction of steam as a function of the tube length and simulation time.

The simulation of an entire start-up procedure is seen in Fig. 6. The pressure is increased after the available free volume in the steam drum is filled with steam and follows the pressure gradient given by the maximum allowable temperature gradient. When the first phase transition is encountered, the water level inside the steam drum rises. The same applies when the second phase transition is experienced. A zoomed image of the boiling in the second top element is seen in Fig. 7.

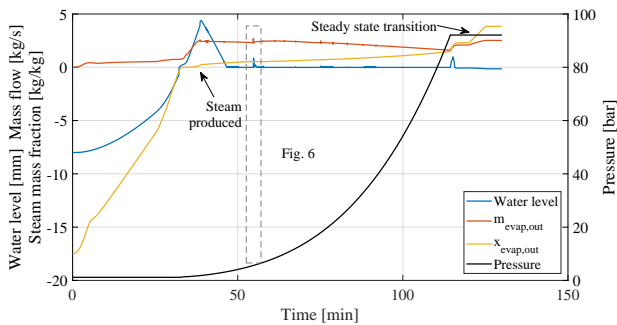


Figure 6: Simulation of a cold start-up procedure. After $P_D = 92$ bar is reached, the system transitions into steady-state.

Analysing Fig. 7 shows that when boiling occurs in the second top element, the fluid expands rapidly to form steam. The gas displaces the liquid in the element, resulting in a rapid local

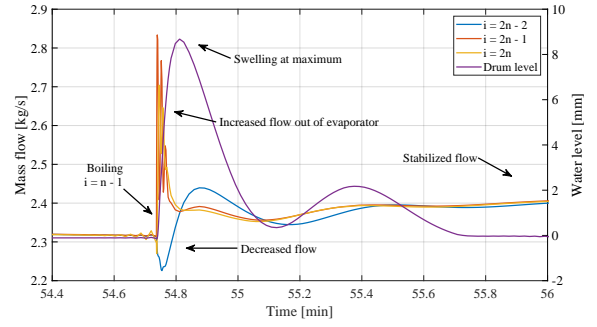


Figure 7: Sudden swelling inside the steam drum when boiling occurs in the second top element. See Fig. 2 for element description.

pressure increase in the element. Since the system is modelled using a homogeneous model with no slip, the liquid is 'pushed' upwards with the produced steam, resulting in increased mass flow. The increased mass flow going out of the element results in an increased mass flow out of the evaporator, causing the water level inside the steam drum to rise. It is worth noting, that the elements located below the boiling elements experience a decreased flow at the same time where the increased flow is experienced. This is due to the fast local pressure increase in the element where boiling is observed.

Chen et al. [25] observed similar phenomena using an experimental approach. During the transition into the two-phase regime, increased velocity is observed, resulting in a larger pressure gradient. The larger pressure gradient forces the system to find another feasible solution, resulting in a lower velocity again. When boiling was observed, Chen et al. [25] observed an increased mass flow for a short period of time. The increased mass flow due to density wave oscillations was observed as a repeating phenomenon. In this work, the increased mass flow due to density wave oscillations is only observed once for every discretized tube element. Chen et al. [25] performed experimental work on a system operating in steady-state with a constant pressure, where the system presented in this work, is dynamic and the pressure increases as a function of time. The system 'pushes through' the dynamic instability phase, eventually resulting in a stable flow, due to the increasing pressure over time.

The mass flow as a function of tube length and time is seen in Fig. 8 and the points represent every time there is a phase transition in the system. It is seen that every time a phase transition occurs, the mass flow increases in the elements placed above the element where boiling occurs. The increased mass flow out of the evaporator is most significant in the first third of the start-up time, due to the lower pressure in the system. When the pressure becomes sufficiently high, the density wave oscillations become less dominating, due to the smoother phase transition.

Shi et al. [26] observed similar phenomena during the phase transition. The authors designed a test facility for a nuclear reactor and observed the dynamic instabilities occurring during the start-up. The authors categorised the flow oscillations as flashing instability, density wave oscillations and Geysering in-

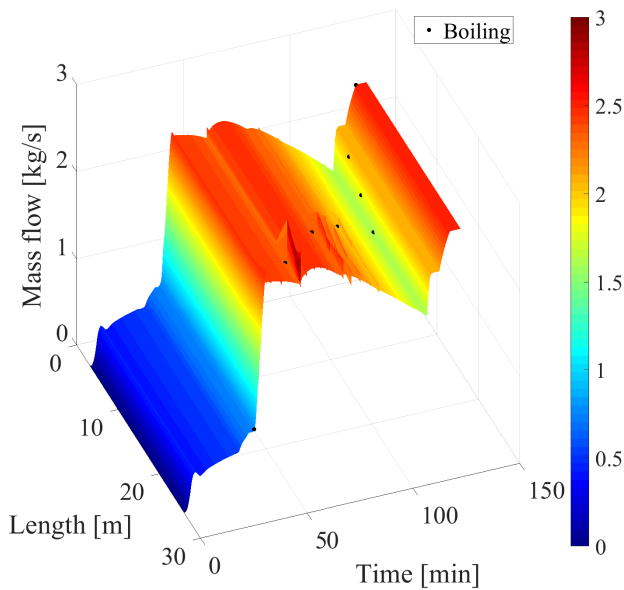


Figure 8: Mass flow in the discretized element as a function of the tube length and simulation time. Every time a phase transition occurs in a tube, an increased flow out of the evaporator is experienced.

stability. When density wave oscillations were observed, a similar oscillating flow pattern was observed.

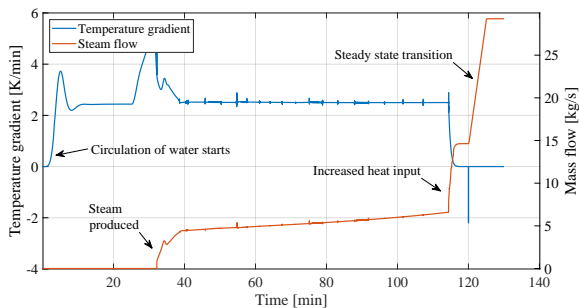


Figure 9: Temperature gradient of the steam drum and steam flow leaving the steam drum as a function of time. When steam is produced, the temperature gradient of the steam drum is controlled using an ideal steam valve.

The temperature gradient of the steam drum, seen in Fig. 9, is controlled using the ideal steam valve, as described in section 2. Before steam is produced, the temperature gradient of the steam drum is a function of the heat input to the furnace. When the free available space in the steam drum is filled with steam, the steam that cannot be stored in the steam drum at the given pressure leaves the steam drum at the desired rate. The steam can leave at any desired rate since the main steam valve is assumed to be ideal. This is seen when steam leaves the steam drum, where a steam mass flow of 5 kg/s is rapidly obtained. This would be difficult to obtain with a real valve following a valve characteristic. When the load is increased, as seen in Fig. 9, the steam flow leaving the steam drum increases. This is also

the case during the transition to steady-state. The steam flow increases during the transition to steady-state, since the maximum operating pressure is reached, and all the steam produced in the evaporator leaves the steam drum.

When steam is produced, the temperature gradient of the steam drum increases rapidly. This is due to the DWOs, experienced at the phase transitions, 'pushing' the hot water, stored in the evaporator tubes, to the steam drum. The mass of water inside the steam drum is rapidly increased during this period, which is also seen in Fig. 6 and this causes the temperature to increase rapidly.

4. Conclusion

A mathematical model describing the dynamic cold start-up procedure of a natural circulation boiler is made. The model takes the subcooling of water into consideration when circulating the water, and special care is taken to resolve the phase transition of the fluid. During the phase transition of water in the discretized element, the steam produced displaces the liquid, resulting in an increased mass flow out of the evaporator. The increased flow leaving the evaporator eventually results in the water level increasing rapidly in the steam drum. The dynamic instabilities encountered when a phase transition is occurring are important to resolve when modelling a natural circulation boiler. The increased mass flow leaving the evaporator when boiling is encountered, may result in a high water level inside the steam, ultimately resulting in a safety shutdown of the plant. Special care has to be taken when modelling a system with a natural circulation boiler since the water entering the evaporator is subcooled due to the geodetic pressure at the bottom of the downcomer tube.

5. Acknowledgements

We would like to thank Aalborg Energie Teknik A/S and their employees for supporting the first author during the development of this model. Without the discussion and help received from these people the project would not have been possible.

This research did not receive any specific grant from funding agencies in the public, commercial, or not-for-profit sectors.

References

- [1] B. Elmegaard, Simulation of Boiler Dynamics: Development, Evaluation and Application of a General Energy System Simulation Tool, Department of Energy Engineering, 1999.
- [2] K. Åström, R. Bell, Drum boiler dynamics, *Automatica* 36 (3) (2000) 363–378. doi:[10.1016/S0005-1098\(99\)00171-5](https://doi.org/10.1016/S0005-1098(99)00171-5).
- [3] E. Adam, J. Marchetti, Dynamic simulation of large boilers with natural recirculation, *Computers and Chemical Engineering* 23 (8) (1999) 1031 – 1040. doi:[https://doi.org/10.1016/S0098-1354\(99\)00269-0](https://doi.org/10.1016/S0098-1354(99)00269-0).
- [4] H. Kim, S. Choi, A model on water level dynamics in natural circulation drum-type boilers, *International Communications in Heat and Mass Transfer* doi:<https://doi.org/10.1016/j.icheatmasstransfer.2004.10.010>.
- [5] A. Sedic, S. Katulic, D. Pavkovic, Dynamic model of a natural water circulation boiler suitable for on-line monitoring of fossil/alternative fuel plants, *Energy Conversion and Management* doi:<https://doi.org/10.1016/j.enconman.2014.06.059>.
- [6] A. Johansen, B. Elmegaard, T. Kristensen, J. Sørensen, Numerical study of evaporators in power plants for improved dynamic flexibility, Ph.D. thesis, DTU Mechanical Engineering (2013).
- [7] Y. Ding, S. Kaka, X. Chen, Dynamic instabilities of boiling two-phase flow in a single horizontal channel, *Experimental Thermal and Fluid Science* 11 (4) (1995) 327 – 342. doi:[https://doi.org/10.1016/0894-1777\(95\)00036-4](https://doi.org/10.1016/0894-1777(95)00036-4).
- [8] F. Alobaid, W. A. K. Al-Maliki, T. Lanz, M. Haaf, A. Brachthuser, B. Eple, I. Zorbach, Dynamic simulation of a municipal solid waste incinerator, *Energy* 149 (2018) 230 – 249. doi:<https://doi.org/10.1016/j.energy.2018.01.170>.
- [9] S. Kakac, B. Bon, A review of two-phase flow dynamic instabilities in tube boiling systems, *International Journal of Heat and Mass Transfer* 51 (3) (2008) 399 – 433. doi:<https://doi.org/10.1016/j.ijheatmasstransfer.2007.09.026>.
- [10] E. Åbro, G. Johansen, Improved void fraction determination by means of multibeam gamma-ray attenuation measurements, *Flow Measurement and Instrumentation* 10 (2) (1999) 99 – 108. doi:[https://doi.org/10.1016/S0955-5986\(98\)00043-0](https://doi.org/10.1016/S0955-5986(98)00043-0).
- [11] R. W. Pike, B. Wilkins Jr., H. C. Ward, Measurement of the void fraction in two-phase flow by x-ray attenuation, *AIChE Journal* 11 (5) (1965) 794–800. doi:[10.1002/aic.690110510](https://doi.org/10.1002/aic.690110510).
- [12] Y. Zhao, Q. Bi, Y. Yuan, H. Lv, Void fraction measurement in steam-water two-phase flow using the gamma ray attenuation under high pressure and high temperature evaporating conditions, *Flow Measurement and Instrumentation* 49 (2016) 18 – 30. doi:<https://doi.org/10.1016/j.flowmeasinst.2016.03.002>.
- [13] E. Nazemi, S. Fegghi, G. Roshani, R. G. Peyvandi, S. Setayeshi, Precise void fraction measurement in two-phase flows independent of the flow regime using gamma-ray attenuation, *Nuclear Engineering and Technology* 48 (1) (2016) 64 – 71. doi:<https://doi.org/10.1016/j.net.2015.09.005>.
- [14] J. Taler, B. Wglowski, D. Taler, T. Sobota, P. Dzierwa, M. Trojan, P. Madejski, M. Pilarczyk, Determination of start-up curves for a boiler with natural circulation based on the analysis of stress distribution in critical pressure components, *Energy* 92 (2015) 153 – 159. doi:<https://doi.org/10.1016/j.energy.2015.03.086>.
- [15] G. W. Ernst Hairer, Syvert Paul Nørsett, Solving Ordinary Differential Equations II. Stiff and Differential-Algebraic Problems, Springer-Verlag, 2002.
- [16] U. M. Ascher, L. R. Petzold, Computer Methods for Ordinary Differential Equations and Differential-Algebraic Equations, 1st Edition, Society for Industrial and Applied Mathematics, Philadelphia, PA, USA, 1998.
- [17] The International Association for the Properties of Water and Steam, [iapws steam tables](http://iapws.org) (1997). URL www.iapws.org
- [18] M. Holmgren, [X steam for matlab](http://www.x-eng.com), downloaded from MathWorks’ File Exchange (2006). URL www.x-eng.com
- [19] International Association for the Properties of Water and Steam, Guide-line on the fast calculation of steam and water properties with the spline-based table look-up method (sbt)IAPWS G13-15.
- [20] J. G. Collier, J. R. Thome, Convective Boiling and Condensation, 3rd Edition, Oxford University Press, 1994.
- [21] P. B. Whalley, Boiling, condensation, and gas-liquid flow, Oxford University Press, 2011.
- [22] Y. A. Cengel, Fundamentals of Thermal-Fluid Sciences, McGraw-Hill, 2002.
- [23] S. Kandlikar, A general correlation for saturated two-phase flow boiling heat transfer inside horizontal and vertical tubes, *Journal of Heat Transfer-Transactions of The ASME* 112 (1990) 219–228.
- [24] K. Sørensen, Dynamic boiler performance: Modelling, simulating and optimizing boilers for dynamic operation, Ph.D. thesis, Institut for Energetik, Aalborg Universitet (2004).
- [25] X. Chen, P. Gao, S. Tan, Z. Yu, C. Chen, An experimental investigation of flow boiling instability in a natural circulation loop, *International Journal of Heat and Mass Transfer* 117 (2018) 1125 – 1134. doi:<https://doi.org/10.1016/j.ijheatmasstransfer.2017.10.076>.
- [26] S. Shi, T. Hibiki, M. Ishii, Startup instability in natural circulation driven nuclear reactors, *Progress in Nuclear Energy* 90 (2016) 140 – 150. doi:<https://doi.org/10.1016/j.pnucene.2016.03.016>.